IOP Publishing Journal of Physics D: Applied Physics

J. Phys. D: Appl. Phys. **51** (2018) 045504 (23pp) https://doi.org/10.1088/1361-6463/aa9f69

Structural, microstructural and electrochemical properties of dispersed-type polymer nanocomposite films

Anil Arya and A L Sharma

Centre for Physical Sciences, Central University of Punjab, Bathinda 151001, Punjab, India

E-mail: alsharmaiitkgp@gmail.com

Received 10 September 2017, revised 1 December 2017
Accepted for publication 5 December 2017
Published 8 January 2018

Abstract

Free-standing solid polymer nanocomposite (PEO–PVC) + $LiPF_6$-TiO_2 films have been prepared through a standard solution-cast technique. The improvement in structural, microstructural and electrochemical properties has been observed on the dispersion of nanofiller in polymer salt complex. X-ray diffraction studies clearly reflect the formation of complex formation, as no corresponding salt peak appeared in the diffractograms. The Fourier transform infrared analysis suggested clear and convincing evidence of polymer–ion, ion–ion and polymer–ion-nanofiller interaction. The highest ionic conductivity of the prepared solid polymer electrolyte (SPE) films is ~5 $\times$ 10^{-5} S cm^{-1} for 7 wt.% TiO_2. The linear sweep voltammetry provides the electrochemical stability window of the prepared SPE films, about ~3.5 V. The ion transference number has been estimated, $t_{ion} = 0.99$ through the DC polarization technique. Dielectric spectroscopic studies were performed to understand the ion transport process in polymer electrolytes. All solid polymer electrolytes possess good thermal stability up to 300 °C. Differential scanning calorimetry analysis confirms the decrease of the melting temperature and signal of glass transition temperature with the addition of nanofiller, which indicates the decrease of crystallinity of the polymer matrix. An absolute correlation between diffusion coefficient (D), ion mobility (μ), number density (n), double-layer capacitance (C_{dl}), glass transition temperature, melting temperature (T_m), free ion area (%) and conductivity (σ) has been observed. A convincing model to study the role of nanofiller in a polymer salt complex has been proposed, which supports the experimental findings. The prepared polymer electrolyte system with significant ionic conductivity, high ionic transference number, and good thermal and voltage stability could be suggested as a potential candidate as electrolyte cum separator for the fabrication of a rechargeable lithium-ion battery system.

Keywords: polymer blend, structural properties, glass transition temperature, transport parameters, transport mechanism

(Some figures may appear in colour only in the online journal)

1. Introduction

In the last two decades, lithium ion batteries (LIBs) have been a widely investigated energy source for portable electronics, because of attractive features such as high energy density, shape mouldability, design flexibility, zero memory loss and high safety. The desirable characteristics of polymer electrolytes for R&D application in LIBs are that they have good compatibility with electrode materials, are leakproof, have a longer shelf life, high capacity and are light weight [1]. The conductivity in solid-state conductors was reported for the first time by Faraday in the 1800s, and later the discovery

of poly(ethylene oxide) (PEO) and alkali metal salt (NaI) systems in the 1970s was made by Wright and co-workers. Then, Armand realized their technological importance due to their flexibility and deformability and introduced the first new class of solid-state ionic conductors (SSICs). Solid polymer electrolytes (SPEs) having high electrical conductivity along with mechanical flexibility, and faster segmental motion of polymer chains makes them the best alternative to liquid electrolytes in electrochemical devices such as supercapacitors, cell phones, LIBs, fuel cells, and smartphones. The liquid electrolytes offer limitations such as chemical reactivity with lithium metal electrodes, leakage, and the need of an additional inert separator for device applications. Furthermore, poor mechanical stability, thermal stability and chemical stability of gelled polymer electrolytes, due to the presence of polar solvents imparting semi-solid/liquid behavior, restricts their use in storage/conversion devices [2–5].

The SPE acts as both the separator and the electrolyte, with the aim of improving the battery's design and reliability [6, 7]. SPEs usually consist of an amorphous high molecular weight polymer matrix and salt with large anion dissolved in it to reduce ion aggregation. The polymer contains ligand coordination to the cations of the salt, and provides the key solvation enthalpy to promote the formation of the polymer electrolyte. The polymer chains consistently create suitable coordinating sites adjacent to the ions; they facilitate the movement of ions via segmental motion. The primary focus of the present study is to improve the ionic conductivity of SPEs, which could be achieved by two means: (1) improvement in polymer chain mobility by suppressing crystallization polymer chains; (2) an increase in a number of free ion charge carriers. The improvement in the polymer chain mobility can be obtained by cross-linking and blending. Of the two possibilities, blending is the most attractive. Polymer blends are obtained by physical mixing of two or more polymers without any chemical reaction between them. This provides superior properties to individual polymer and can be easily controlled by varying the composition of the polymer used [8–10].

A polymer blending technique is the best approach to develop the new polymeric materials for application prospects. Recently, much effort has been devoted to enhance the electrochemical and mechanical properties in blend polymer electrolyte (BPE) membranes, such as PEO–PAN [11], PVdF–PEO [12], PEO–PVdF [13], PVA–PEO [14], PEO–PEG [15], PVA–PVP [16], PVC–PEMA [17], PEO–PVP [18] and PVC–PEO [19–21]. Various strategies are considered for enhancing the ionic conductivity of SPEs, such as the addition of plasticizers, organic liquids, nanofiller and organic clay. To achieve high ionic conductivity and mechanical properties, the doping of nano-sized fillers/plasticizers having large surface area is an effective approach. This also increases the amorphous content, which results in faster transport of ions by coordinating sites of the host polymer. The addition of nanofiller with high dielectric constant and high thermal stability improves the mechanical, thermal, and electrochemical properties of the electrolyte due to the increase in free volume and leads to increased mobility of polymer chains and a reduction in crystallinity [22–34].

To date, the high molecular weight PEO-based polymeric electrolytes have been widely researched due to their semi-crystalline nature and the presence of the ether group, which supports faster ionic transport due to beneficial polymer flexibility [35, 36]. The host polymer is PEO containing ether group (–Ö–), which provides coordinating sites to cation (Li^+), and Li^+ acts as Lewis acid. Hence, it can easily form a complex with many alkali salts and provides a direct path for cation migration due to the presence of the ether group $(–CH_2–CH_2–Ö–)_n$ in the polymer backbone. However, in PEO because of the presence of C–C, C–O and C–H bonds, the low reactivity provides better chemical and electrochemical stability, but poor ionic conductivity and thermal stability [18]. To overcome the limitation of lower ionic conductivity and limited working temperature (100 °C) in PEO due to low melting temperature (65 °C), polyvinyl chloride (PVC) has been chosen as a partner to PEO for synthesizing BPE, which permits faster ion migration than the semi-crystalline polymer. In addition, this supports the superior mechanical and thermal properties of the other polymers. PVC ($(C_2H_3Cl)_n$) has an amorphous structure, resistant to oxidative reactions, a high melting temperature (~260 °C) and acts as an excellent mechanical stiffener. Also, the blending of PVC with PEO provides a wide temperature range of operation (~200 °C) compared to pure PEO, which is a vital requirement for energy-storage devices [37]. The salt is chosen due to its unique properties such as good ionic conductivity, smaller cation size (~0.76 Å), bulky anion (~2 Å) and low lattice energy. Other salts with a large anion such as LiTFSI and LiBETI are also available, but corrosion with the aluminum collector limits their use in commercial devices [38]. So, $LiPF_6$ is the best salt as it provides an adequate balance of electrical, mechanical and thermal properties. The Lewis acid group of inert nanofiller (Ti^{+2}) may compete with Lewis acid Li^+ for the formation of a complex with salt. These interactions result in lowering the ion coupling, by structural modification and promote more salt dissociation for free ions. As polymer phase is the medium of transport of ions and nanofiller, interaction with polymer phase affects polymer chain stiffness. Also, there may be the direct interaction of nanofiller with the PEO, cation, and anion due to a higher dielectric constant of TiO_2 ($\varepsilon = 85$) than PEO ($\varepsilon \sim 5$) [39]. Figure 1 displays the molecular structures of the materials used in the present study.

Among the nano-sized ceramic fillers explored recently, TiO_2 seems to be the most promising candidate to increase the ionic conductivity due to its high Lewis-acid character compared to other commonly used ceramic fillers (such as Al_2O_3, SiO_2, and ZrO_2). Scrosati *et al* [27], also studied the PEO–$LiClO_4$ complexes with TiO_2 and Al_2O_3 ceramic fillers and reported that TiO_2 additionally exhibited the greatest enhancement in ionic conductivity. Chung *et al* [40] studied the effects of TiO_2, Al_2O_3, and SiO_2 in PEO–$LiClO_4$ polymer electrolyte and identified TiO_2 as the filler with the greatest enhancement in ionic conductivity due to lowering of interactions between the polymer chain and Li^+ ions. Although it has been

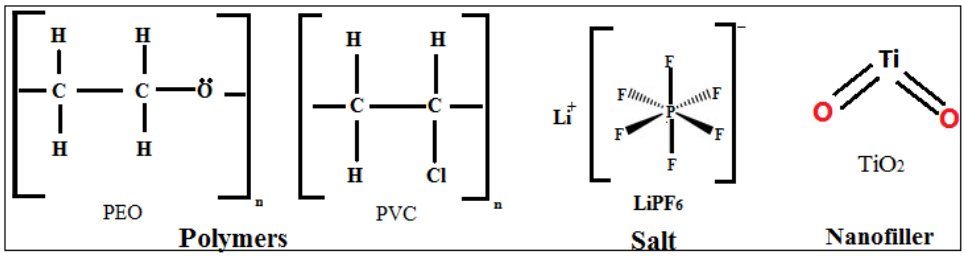

Figure 1. Molecular structure of materials.

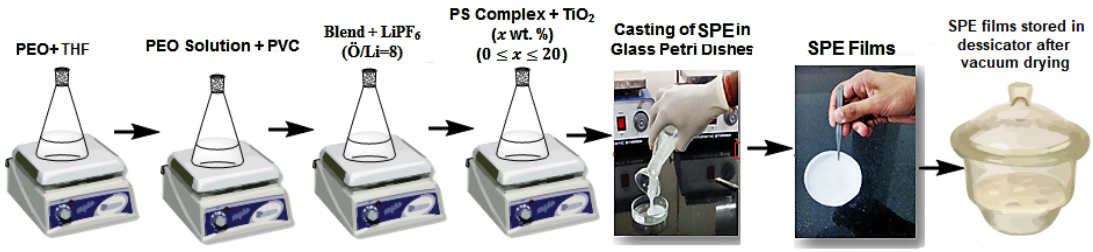

Figure 2. Flow chart of solution-cast technique.

compared by taking different nanofiller of the same concentration with polymer salt (PS) complex and found that the conductivity maxima appear to be for Er_2O_3, sample preparation for low concentration of Er_2O_3 is not so easy. Therefore, the selection of TiO_2 as nanofillers seems to be more appropriate for better study at varying concentrations and in view of the optimization of nanofiller concentrations [41]. Vignarooban *et al* [42] reported the enhancement of ionic conductivity of poly(ethylene oxide)–lithium trifluoromethanesulfonate ($LiCF_3SO_3$ or LiTf)-based polymer electrolyte by incorporating TiO_2 nanofiller. To the best of our knowledge, there is no study available in the literature on the ionic conductivity enhancement of PEO–PVC + $LiPF_6$-based SPE on the addition of nano-sized TiO_2 ceramic filler. Contextually, this is the first report with $LiPF_6$ salt for PEO–PVC blend-based SPE. The present work discusses the preparation of SPE with different nanofiller content by a universal solution-cast technique. The structural, thermal, electrical and transport properties of polymer nanocomposites have been investigated. Finally, a self-proposed ion transport mechanism is established to support the experimental data.

2. Experimental

2.1. Materials

All the SPE samples were prepared by a standard solution-cast technique. The SPE system involved the use of PEO and PVC with average molecular weights of 1×10^6 (Sigma-Aldrich), and 6×10^4, respectively. Salt $LiPF_6$ and titanium oxide (TiO_2) were acquired from Sigma-Aldrich. Anhydrous tetrahydrofuran (THF), used as a solvent, was purchased from Sigma-Aldrich.

2.2. Preparation of SPE

All the SPE films were prepared by a standard solution-cast technique reported elsewhere [7]. A snapshot of the method is shown in the flow chart/diagram (figure 2). The PEO was stirred in THF (15 ml) for 8 h and then PVC was added to the solution and again stirred to carry out physical blending for 10 h. Subsequently, an optimized amount of (stoichiometric) $LiPF_6$ (Ö/Li = 8) was added to the polymer blend and stirred mechanically for 12 h to allow homogenous mixing and complexation. Next, TiO_2 nanofiller was added to the polymer salt complex solution in different x wt.% concentration ($0 \leqslant x \leqslant 20$; x refers to nanofiller wt.% concentration) and stirred for 12 h. Then, the obtained solution was sonicated for 30 min for homogenous mixing of the nanofiller. The prepared polymer nanocomposite solutions were casted in petri dishes and kept at 60 °C for 24 h in a vacuum oven. Finally, the free-standing polymer films were peeled off the petri dishes and stored in a vacuum desiccator with silica gel to avoid any moisture content.

2.3. Characterization

X-ray diffraction (XRD) is the most useful method for investigating the structural properties and crystallinity of the polymer matrix. The XRD was recorded with Cu-K_α radiation ($\lambda = 1.54$ Å) in the Bragg angle range (2θ) from 10°–60° with a scan rate of 2° min^{-1}. Field emission scanning electron microscopy (FESEM) was used to study the surface morphology (FESEM: Carl Zeiss) and taken in a high vacuum after sputtering the samples with gold to prepare conductive surfaces. The Fourier transform infrared (FTIR) spectra were recorded using a Bruker Tensor 27 (Model: NEXUS –870) in absorbance mode over the wavenumber region from 600–4000 cm^{-1} with a resolution of 4 cm^{-1}. FTIR is performed to probe the presence of microscopic interactions between polymer–ion, ion–ion and polymer–ion nanofiller. The electrical conductivity of the SPE films was evaluated using an electrochemical analyzer (CHI 760; USA) over the frequency range from 1 Hz–1 MHz at a signal level of 10 mV by sandwiching the SPE between two stainless steel (SS) electrodes

at room temperature. The intercept between the semi-circle at high frequency and the tilted spike at low frequency were taken as the bulk resistance (R_b). The ionic conductivity (σ) value was obtained using equation (1):

$$\sigma_{dc} = \frac{1}{R_b}\frac{t}{A}, \tag{1}$$

where t is the thickness (cm) of the polymer film, R_b is the bulk resistance (Ω) and A is the area (cm^2) of the working electrode. The real (Z') and imaginary (Z'') parts of the complex impedance were used to calculate the real (ε'), imaginary (ε'') parts of the permittivity and AC conductivity (σ_{ac}). The total ionic transference number (t_{ion}) was obtained by sandwiching polymer electrolyte film between SS blocking electrodes and a fixed DC voltage of 0.05 V was applied across the SS|SPE|SS cell. Ion transference numbers of the SPE were evaluated using equation (2) on the *SS|SPE|SS* cell:

$$t_{ion} = \left(\frac{I_t - I_e}{I_t}\right) \times 100, \tag{2}$$

where I_t and I_e are the total and residual current, respectively.

The linear sweep voltammetry (LSV) was characterized to obtain the working voltage window of the electrolyte. The thermal stability of the synthesized SPE films was investigated using thermogravimetric analysis (TGA—SHIMDZU–DTG-60H) under dynamic temperature conditions from 30 °C–600 °C, in a controlled nitrogen atmosphere at a constant heating scan rate of 10 °C min^{-1}. Differential scanning calorimetry (DSC) measurements were performed to find the glass transition temperature and crystallinity of all SPEs with a heating rate of 10 °C min^{-1} from −100 °C°100 °C under N_2/Ar atmosphere (DSC-Sirius 3500). SPE films with the weight of 8–10 mg were sealed in aluminum pans, and an empty aluminum pan was used as a reference.

3. Results

3.1. XRD analysis

Figure 3 represents the XRD patterns of a PEO–PVC polymer blend and a blend polymer salt complex with different concentrations of TiO_2. An XRD pattern of the PEO–PVC film exhibits two partially crystalline characteristic diffraction peaks at $2\theta = 19.30°$ and 23.47° for PEO relevant to the [1 2 0] and [0 3 2] + [1 1 2] planes [43]. The above inspection shows the presence of multiphase character consisting of both crystalline and amorphous nature. In contrast, the addition of salt ($LiPF_6$) to the polymer blend shows a shift in peaks toward a lower angle side 18.67° and 23.26°. Also, the peak intensity decreases, which suggests the reduction in the crystallinity of the polymer blend [44]. It may be due to the strong interaction of cation (Li^+) with the electron-rich ether group of the polymer host. It can be concluded that the amorphous phase is enhanced by the accommodation of the lithium ion (Li^+) in the polymer backbone. The above analysis is also in correlation with that given by Hodge *et al* [45], between the degree of crystallinity and peak intensity, which states that higher crystallinity is associated with greater peak intensity.

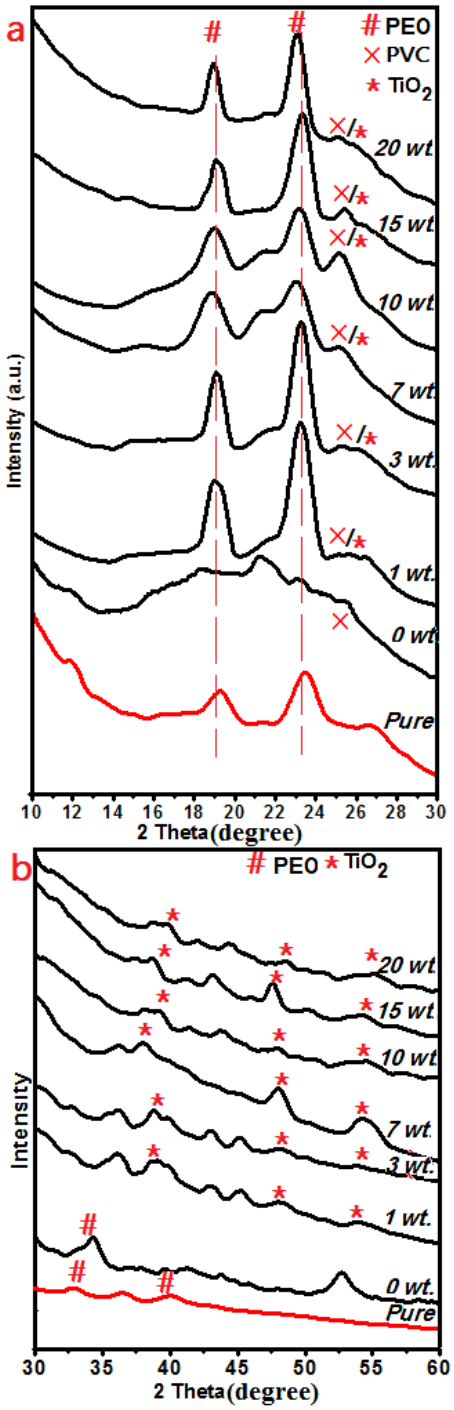

Figure 3. XRD patterns of various SPEs with TiO_2 nanofiller.

The absence of a peak corresponding to $LiPF_6$ reveals complete dissociation of the salt in the BPE. Besides these crystalline peaks, the broad hump near 25° is also observed, and it arises from the amorphous phase of the PVC [46, 47]. The sharpness of diffraction peaks corresponding to PVC is the same in all samples, which suggests that salt interacts with PEO and the amorphous phase formation occurs due to disruption of the crystalline chain arrangement. The addition of nanofiller has brought noticeable changes in the peaks with a shift in position and broadening. The XRD pattern of TiO_2-added SPE (figures 3(c)–(h)) exhibits lower intensity peaks

Table 1. Values of Bragg angle 2θ, Basal spacing (d), FWHM (β), crystallite size (L) and inter-chain separation (R) corresponding to 120 and 112/0.32 reflection planes of PEO in PEO–PVC + $LiPF_6 - x$ wt.% TiO_2 nanocomposite films.

Sample code	2θ (degree)	d (Å)	R (Å)	$\beta \times 10^3$ (radians)	L (nm)
PEO 120 reflection plane parameters					
PEO–PVC blend	19.23	4.61	5.76	19.49	7.79
$x = 0$	18.45	4.80	6.00	13.75	10.60
$x = 1$	19.07	4.65	5.81	16.88	8.65
$x = 3$	19.16	4.62	5.78	12.88	11.33
$x = 7$	18.91	4.68	5.85	24.19	6.03
$x = 10$	18.98	4.67	5.86	20.18	7.23
$x = 15$	19.16	4.62	5.78	14.27	10.23
$x = 20$	19.10	4.64	5.79	16.01	9.12
PEO 112/0.32 reflection plane parameters					
PEO–PVC blend	11.74	3.78	4.72	20.71	7.10
$x = 0$	11.59	3.83	4.78	37.24	3.94
$x = 1$	11.65	3.81	4.76	18.97	7.75
$x = 3$	11.61	3.82	4.78	16.18	9.08
$x = 7$	11.55	3.84	4.80	16.36	8.98
$x = 10$	11.56	3.84	4.80	18.27	8.04
$x = 15$	11.71	3.79	4.73	17.92	8.20
$x = 20$	11.74	3.78	4.72	22.97	6.40

located at 26.70°, 36.80°, 45.05° and 54.8°, respective to the [1 0 1], [1 1 2], [2 0 0] and [2 1 1] planes [44]. The strong diffraction peaks at $2\theta = 25.4°$ and 48° confirm the TiO_2 anatase structure and absence of a broad diffraction peak on the addition of the nanofiller, as evidenced by the modification in the polymer salt matrix.

The d-spacing between the diffraction planes was obtained using Bragg's formula $2d\sin\theta = n\lambda$, crystallite size L of PEO crystalline from Sherrer's equation $L = 0.94\lambda/\beta\cos\theta$ and interchain separation (R) using the equation $R = 5\lambda/8\sin\theta$, and the determined values are shown in table 1. It is found that the Basal spacing and crystallite size change with the addition of the nanofiller and may be attributed to the polymer–ion-nanofiller interaction. The increase of interchain separation (R) evidences the increase of the amorphous content or free volume after the addition of the nanofiller owing to the nanofiller interaction with the polymer chains. This increase of the free volume promotes the faster ion migration due to the the faster segmental motion of the polymer chains. The addition of nanofiller makes the polymer chains more flexible by reducing the covalent bonding between the polymer chains, which leads to the faster polymer chain segmental motion.

The disappearance of some small-intensity peaks in the polymer matrix suggests the presence of strong interaction between the polymer-salt and nanofiller. The TiO_2 nanofiller-based SPEs also display a slight shift compared to the polymer salt complex and polymer blend, which is evidence of amorphous phase formation due to coordinating interaction between a surface group of nanofiller and the polymer host. The above coordinating interaction increases the polymer segmental motion or polymer flexibility, which supports fast ion transport and directly evidences an increase of ionic mobility and hence ionic conductivity.

3.2. FESEM analysis

The electrical properties of SPE films are completely associated with the surface morphology and a smoother, more dense film often facilitates faster transport of ions, since it will be more ordered and less porous. To understand the role of salt and nanofiller on surface properties, specific effort has been made to observe the morphologies of the blended polymer electrolyte system using FESEM.

Figure 4 depicts the FESEM of the free-standing SPE films. The rough, interconnected surface of the salt-free blend polymer (PEO–PVC) displays the fundamental nature of the polymer and depends on the interaction as well as evaporation rate of the solvent in blend polymer. A remarkable difference in the surface roughness and texture of the polymer film on the addition of salt is evidenced, as shown in figure 4(b). This irregular appearance of the film confirms polymer salt complex formation. Now, the addition of even a small concentration of nanofiller improves the surface roughness, and the interlining of grain boundaries is seen in the structure (figure 4(c)). The addition of nanofiller even at low wt.% concentration has modified the blend-based free-standing polymer film surface morphology, and a smooth surface of the polymer with nanofiller can be seen (figure 4(e)) [48]. The appearance of dark regions in the micrograph might be due to the continuous growth of the amorphous region of the polymer blend and this region increases with the interruption of the crystallite in the presence of the TiO_2 nanofiller [49]. The smooth surface of the sample reveals that polymer salt has good compatibility with nanofiller and is linked with high amorphous content in the polymer electrolyte. The smooth and homogenous morphology of SPE films with high nanofiller content is evidence of lowering of the crystallinity due to a constraint on the chain reorganization tendency and facilitates rapid ion migration. The high amorphous content enables faster ionic transport by providing an easy path for ion migration and high mobility along with the enhanced flexibility of the films. It is anticipated from the above that the optimized morphology of the polymer film may be reflected in the enhanced electrochemical behavior of the SPE in the LIB (see the following section).

Energy-dispersive x-ray spectroscopy (EDS) mapping is an appropriate tool to study the nanofiller dispersion inside the polymer electrolyte system. FESEM/EDS mapping was also implemented to investigate the presence and distribution of the nanofiller in the polymer matrix. The distribution of Ti atoms was visualized by the EDS elemental mapping of Ti atoms. As expected, the uniform distribution was obtained from nanofiller content, and some agglomeration was observed for high nanofiller content. As can be seen in figure 5, polymer matrix with 7 wt.% nanofiller content in EDS mapping shows uniform/homogenous distribution over the whole surface, as indicated by the red color and this indicates that the TiO_2 particles were well dispersed in the polymer matrix. All three figures show almost identical mapping of the Ti, which reveals

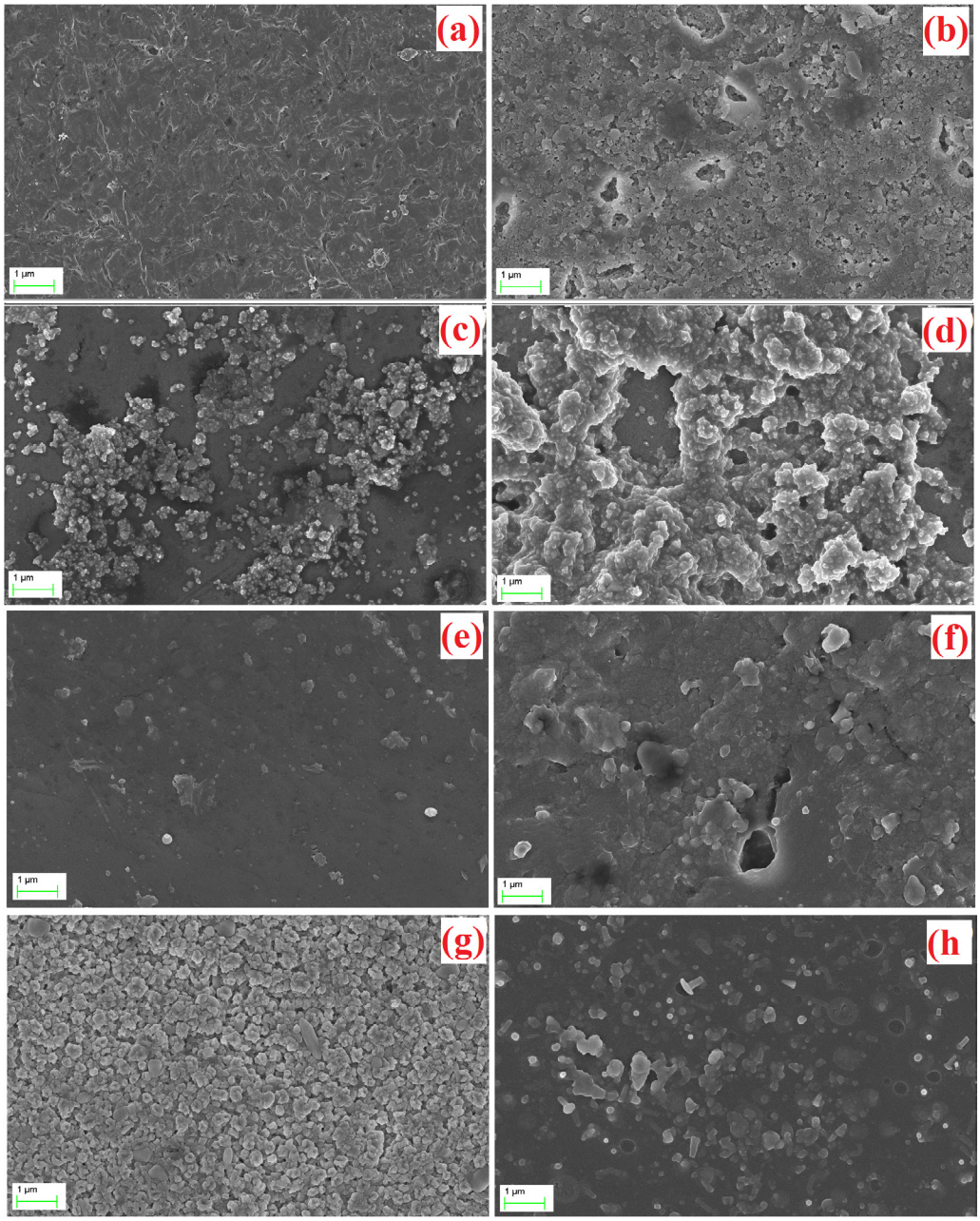

Figure 4. FESEM micrograph of SPE films comprising: (a) host blend polymer and (PEO–PVC)-$LIPF_6$ + x wt.% TiO_2 nanofiller, (b) $x = 0$, (c) $x = 1$, (d) $x = 3$, (e) $x = 7$, (f) $x = 10$, (g) $x = 15$, (h) $x = 20$.

that the nanofiller is mixed properly in the polymer matrix. In addition, it is remarkable that the resulting TiO_2-added SPE membrane is semi-transparent and free-standing (figure 2).

3.3. FTIR analysis

FTIR has proved to be highly effective for investing various interactions such as polymer–ion interaction, ion–ion interaction and polymer–ion-filler interaction. FTIR also confirm the presence of complex formation and demonstrates interaction among different constituents of the polymer matrix. Absorption changes the frequency of stretching and deforming vibrations of these groups and band shift occurs w.r.t. wavenumber, which provides direct evidence of interaction occurring in the polymer matrix system by the addition of nanofiller.

Figure 6 shows the FTIR absorbance spectra of the (PEO–PVC)-$LIPF_6$ + x wt.% TiO_2 ($0 \leqslant x \leqslant 20$)-based system in the wavenumber region 600–3000 cm^{-1} and the band assignment is shown in table 2. The blend PEO–PVC spectrum shows various absorption bands as a fingerprint region (shown by a dotted line) in the region between 600 and 1500 cm^{-1}. The characteristic absorption bands observed in the FTIR spectrum at the wavenumbers ~620, ~845, ~958, ~1080, ~1250, ~1666, ~2880 and 2914 cm^{-1} are attributed to C–Cl_{st}, $\nu_s(PF_6^-)$, trans (C–H) wagging, $t(CH_2)_s$, $\tau(CH_2)_s$, υ(C=O), $\nu_s(CH_2)$ and $\nu_a(CH_2)$, respectively [5, 50]. Most of the bands located at 1250, 1320, 1360, 1398, 1435 and 1465 cm^{-1} are attributed to twisting $(CH_2)_s$, stretching (CH_2), symmetric CH_2 wagging, asymmetric $(CH_2)_a$ wagging, deformation $(CH_2)_s$ and 1465 bending $(CH_2)_a$, respectively exhibited by PEO [36]. The CH_2

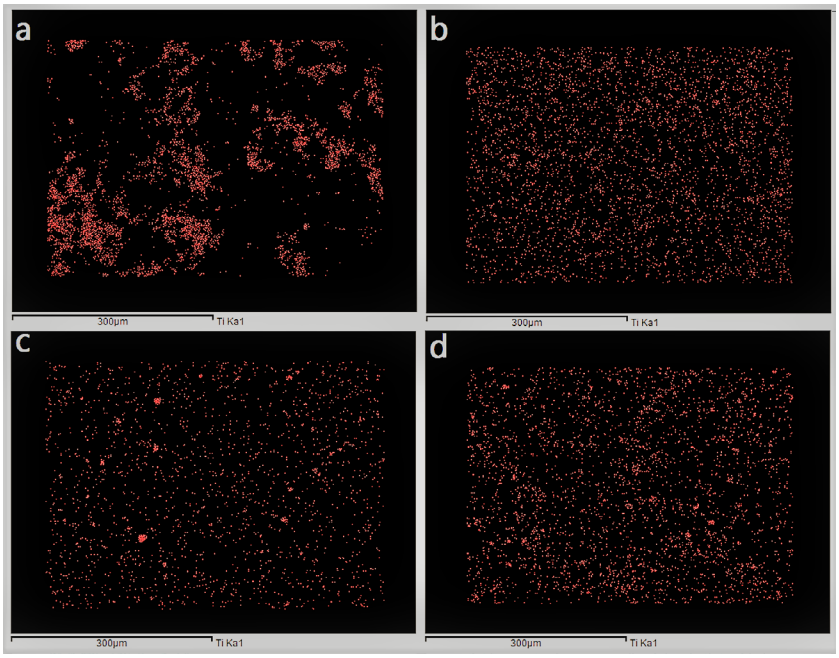

Figure 5. Elemental mapping results of Ti atoms in SPEs for x wt.% nanofiller: (a) $x = 3$, (b) $x = 7$, (c) $x = 10$, (d) $x = 15$.

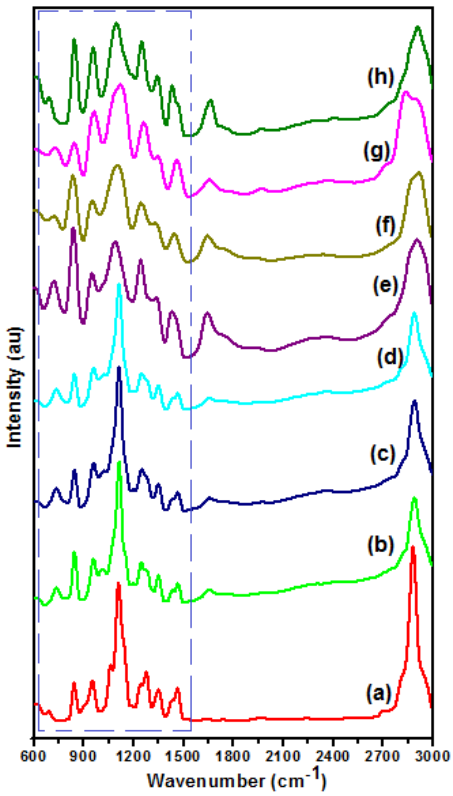

Figure 6. FTIR spectra of: (a) blend polymer and (PEO–PVC)-$LIPF_6 + x$ wt.% TiO_2 films, (b) $x = 0$, (c) $x = 1$, (d) $x = 3$, (e) $x = 7$, (f) $x = 10$, (g) $x = 15$, (h) $x = 20$.

stretching mode also undergoes some variations, which result in the decreased intensity and peak broadening in the range 2850–2950 cm^{-1} with the addition of nanofiller. The peaks appearing near 720 cm^{-1} correspond to the C–Cl stretching mode and at 1060 cm^{-1} are assigned to the (C–C) stretching mode of PVC. The absorption peak located near 958 cm^{-1} corresponds to the *cis* CH wagging and *trans* CH wagging mode of PVC, respectively. The bands present near 958, 1190 and 1254 cm^{-1} are assigned to the CH wagging, CH_2 twisting and CH_2 rocking mode of PVC, respectively [20, 51]. A peak was observed at 1060 cm^{-1} in the PEO–PVC blend associated with the crystalline structure and peak intensity decreases after the addition of salt (figure 6(b)). Further addition of nanofiller demonstrates that it disappeared, indicating the reduction in crystallinity (figures 6(c)–(h)) [52]. In the observed spectra, there are no distinct bands corresponding to TiO_2 nanofiller. The characteristic peaks of pure PEO, (1114 and 1350 cm^{-1}), are shifted to 1112 and 1349 cm^{-1} for the PEO–PVC blend. Furthermore, the characteristic peaks of pure PVC (696 and 1240 cm^{-1}), are shifted to 731 and 1245 cm^{-1} for the PEO–PVC blend system and the above analysis in terms of peak shift evidences the complexation of the PEO–PVC blend. Any interaction of (PF_6^-) anion changes its symmetry from the O_h point group to C_{3v} or C_{2v} and changes in the absorption mode of the polymer matrix are evidenced in the FTIR spectrum between 600 and 1500 cm^{-1}. The effect of the nanofiller on the peak pattern in terms of asymmetry and peak position has been recorded in table 2.

3.3.1. Polymer–ion interaction. The characteristic absorption peak of the host polymer PEO near 1110 cm^{-1} is attributed to the C–O–C symmetric stretching mode involving ether oxygen of PEO and provides direct evidence of complexation owing to the interaction of the ether group of the polymer chain with cation (figure 7). Table 2 shows the shift in the C–O–C band occurring at 1114 cm^{-1} towards a lower wavenumber side to 1112 cm^{-1} on the addition of salt in the polymer blend matrix. This shift of peak towards a lower wavenumber side is strong evidence of cation coordination (Li^+) at the electron-rich ether group of PEO. The variations in the intensity, shape,

Table 2. FTIR band identification and assignment in SPE films (PEO–PVC)-LIPF$_6$ + x wt.% TiO$_2$ ($0 \leqslant x \leqslant 20$).

PEO–PVC	$x = 0$	$x = 1$	$x = 3$	$x = 7$	$x = 10$	$x = 15$	$x = 20$	Band assignment	Ref.
620	617	625	618	620	623	610	616	(C–Cl) st.	[20]
696	731	733	732	727	729	7729	690		
844	844	841	842	846	842	842	842	CH_2 rocking/PF_6^-	[50]
951	956	956	958	960	958	962	958	*trans* $(C–H)_w$	[51]
1114	1112	1112	1112	1097	1107	1122	1098	$\nu(COC)_{s/a}$	[4, 50]
1240	1245	1244	1246	1247	1253	1259	1247	CH rocking/$\tau(CH_2)_s$	[20]
1350	1349	1345	1342	1338	1339	1343	1343	$w(CH_2)_s$	[36]
1434	1426	1429	1432	1434	1435	1438	1429	$\delta(CH_2)_s$	[46]
1467	1467	1463	1462	1466	1457	1458	1471	$\delta(CH_2)_a$	[46, 54]
2888	2885	2884	2883	2895	2883	2885	2881	$\nu(CH_2)_s$	[5]
2914	2910	2909	2903	2918	2919	2921	2911	$\nu(CH_2)_a$	[5]

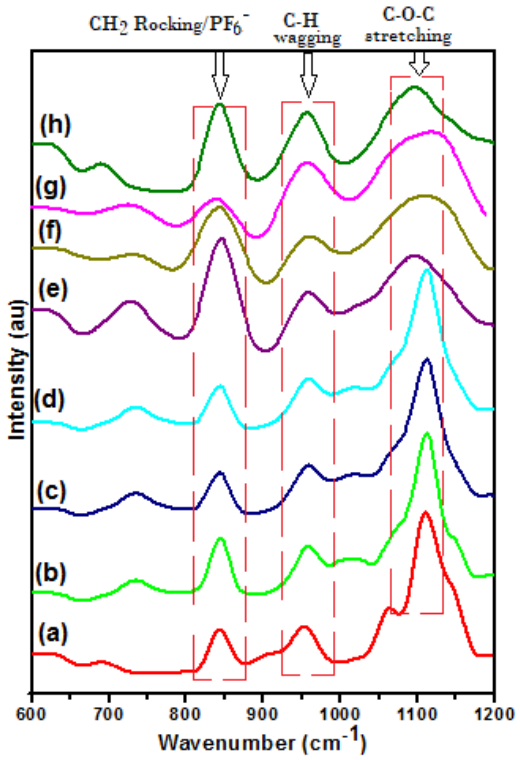

Figure 7. Variation in C–O–C peak of PEO in SPE films: (a) host blend polymer and (PEO–PVC)-LIPF$_6$ + x wt.% TiO$_2$ films, (b) $x = 0$, (c) $x = 1$, (d) $x = 3$, (e) $x = 7$, (f) $x = 10$, (g) $x = 15$, (h) $x = 20$.

and position of the C–O–C symmetric/asymmetric stretching mode were associated with the polymer–LiPF$_6$ interactions, and dependence of the vibrational peaks of C–O–C on the filler concentrations were clarified in the FTIR spectra. The peak broadening and decrease in intensity with the addition of nanofiller reveal the weakening of the C–O–C bond due to interaction with –C=Ö– as an active site for Li^+ coordination (figures 7(c)–(h)). Figures 7(a)–(h) show the spectral pattern of the hexafluorophosphate (PF_6^-) group with octahedral symmetry (O_h) in the SPE films. Any possible coordination of the PF_6^- group with cation usually results in lowering of the PF_6^- group symmetry from the O_h point group to $C_{3\upsilon}$ or $C_{2\upsilon}$ depending on the nature of the coordination that the PF_6^- group possesses (tridentate/bidentate) with cations (Li^+) and other such active sites having Lewis-acid character. Nanofiller addition in the polymer salt matrix may lead to the interaction of nanofiller with the anions (PF_6^-), and changes are evidenced regarding the shift in peak. Also, the profile of the C–H stretching mode near 951 cm^{-1} in the polymer blend shifts to a higher wavenumber side on the addition of salt, suggesting the firm interaction of the polymer with cation. The correlation with electrical conductivity and study of more interaction on the addition of nanofiller is described in a later section.

3.3.2. Ion–ion interaction. The standard internal vibrational mode of the PF_6^- anion in SPE films has been observed in wavenumber region 820–860 cm^{-1} and this demonstrates asymmetry in the peak, as is clearly visible in the polymer salt film (figure 8(a)). This asymmetry in the $\upsilon_3(t_{1u})$ mode is the result of degeneracy ($O_h \rightarrow C_{3\upsilon}$) arising due to the simultaneous presence of more than two components i.e. free ion and ion pairs and is confirmed by ion–ion interaction. This causes a change in the free anion area of the nanofiller-based system compared to the polymer salt system. So, to study the above degeneracy and presence of both components, deconvolution of the PF_6^- anion peak is done for qualitative and quantitative analysis using Peak Fit (V 4.02) software with Voigt Amp profile. The best fit is said to be measured by the correlation coefficient (r^2). A quantitative estimation of the fraction free ion and ion pair in the deconvoluted pattern is obtained using equations (3) and (4):

$$\text{Fraction of free anion} = \frac{\text{Area of free ion peak}}{\text{Total peak area}} \tag{3}$$

and

$$\text{Fraction of ion pair} = \frac{\text{Area of ion pair peak}}{\text{Total peak area}}. \tag{4}$$

The deconvoluted pattern of SPE films with different filler concentration is displayed in figure 8. The deconvoluted pattern appearing in PS film shows two distinct peaks, one at a lower wavenumber and the other at a high wavenumber. It is general convention that the peak at the lower wavenumber is assigned to free PF_6^- anions, which do not directly interact with the lithium cations, and at the higher wavenumber is due to $Li^+ - PF_6^-$ contact ion pairs [53]. In the case of PS film (figure 8(a)), free ion peak is located at 835 cm^{-1} and ion pair at 847 cm^{-1} owing to the peak asymmetry. The deconvoluted

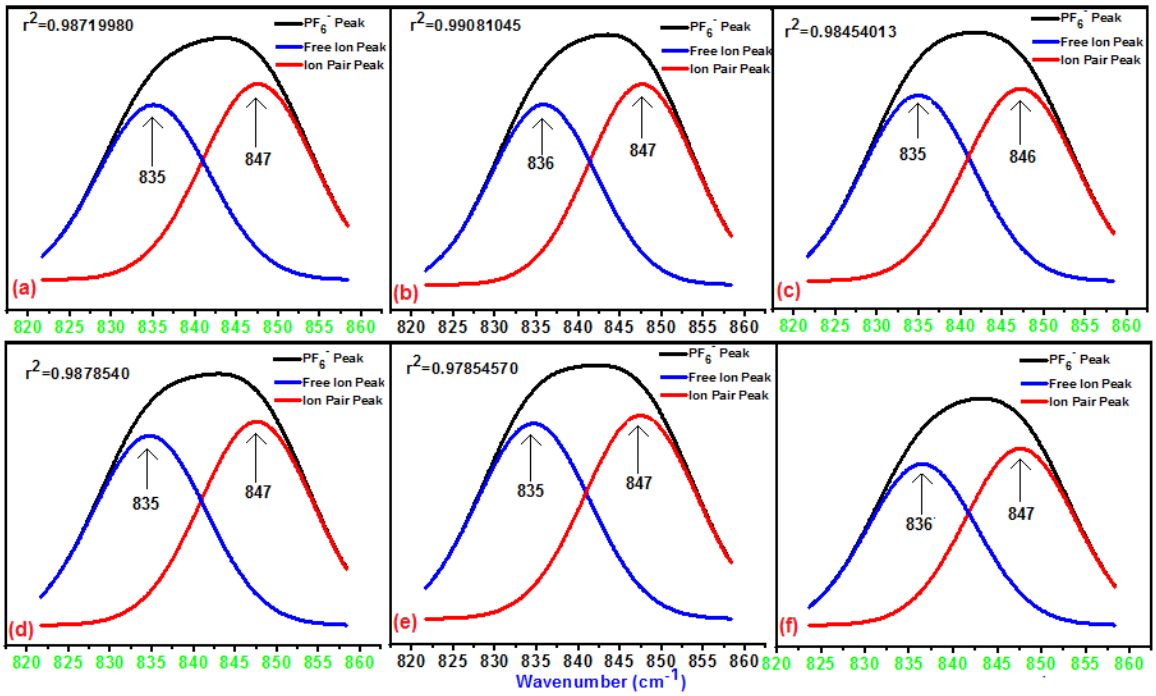

Figure 8. Deconvoluted pattern of hexafluorophosphate (PF_6^-) band at $\vartheta = 840\,cm^{-1}$ showing contribution of free ion and ion pair in (PEO–PVC)-LIPF$_6$ + x wt.% TiO_2 films: (a) $x = 0$, (b) $x = 3$, (c) $x = 7$, (d) $x = 10$, (e) $x = 15$, (g) $x = 20$.

pattern for SPEs depicts changing profile of free ion and ion pair peak in terms of change and shift in position with the addition of nanofiller [54].

A comparison of the free ion area and ion pair area from table 3 shows a relatively higher free ion area for 7 wt.% and 15 wt.%. This increase in area may be attributed to the release of more free charge carriers from anion PF_6^- and it shows the presence of the strong interaction of nanofiller with salt. The increase in free anion concentration results in the movement of free cation concentration, which does not reflect in the mid-IR region. The decrease in the free anion area at high nanofiller content may be due to the trapping of cations in nanofiller clusters and blockage of the conduction path provided by polymer chains [55]. A high degree of ionic dissociation is achieved for 7 wt.% and 15 wt.% nanofiller content. This suggests that the extent of interaction of the lithium cations and the −Ö− groups provides more successful hopping and coordinating sites to the lithium cations, resulting in an enhancement of the number of free charge carriers. In the next section, more probable interactions with the nanofiller addition such as polymer–ion-nanofiller are elaborated upon.

3.3.3. Polymer–ion-nanofiller interaction. The effect of nanofiller addition in polymer salt complex results in a change in band profile of the polymer matrix. Also, the effect of nanofiller is seen on the polymer–ion and ion–ion interaction in SPE films. Figure 9 shows the FTIR spectra in wavenumber range 1240–1480 cm^{-1}. It can be concluded that the various absorption bands of the complex (PEO–PVC)-LIPF$_6$ + x wt.% TiO_2 ($0 \leqslant x \leqslant 20$) are influenced by the addition of TiO_2 nanofiller.

The main bands present at 1280, 1350, 1434 and 1467 cm^{-1} are attributed to twisting $(CH_2)_s$, symmetric CH_2, wagging, deformation $(CH_2)_s$ and bending $(CH_2)_a$, respectively. Figure 9 shows variation in the $\tau(CH_2)_s$ twisting mode of PEO with nanofiller located at 1280 cm^{-1}. The change in vibrational bands on the addition of nanofiller shows that the nanofiller plays an effective role in the polymer salt matrix and interaction occurring between polymer–ion and polymer–ion is evidenced [36, 56]. The intense CH_2 deformation at 1434 cm^{-1} for the blend PEO-PVC shifted to 1434 cm^{-1} on the addition of salt and after the addition of filler from ($0 \leqslant x \leqslant 20$) the shift in the peak is 1426, 1429, 1432, 1434, 1435, 1438 and 1429 cm^{-1}, respectively [4]. This change in wavenumber results in a change in bond length and confirms the complex formation in the SPE films [57, 58]. The CH_2 wagging mode of PEO located at 1350 cm^{-1} is shifted to 1349 cm^{-1} on the addition of salt. The effect of nanofiller was observed on vibration modes in FTIR spectra in terms of the decrease in intensity of the absorption peaks and broadening with shifting in the band profile. The change in the frequency, broadening and intensity depends on the interactions of the polymer matrix with filler and surroundings in polymer nanocomposite (PNC) films [51].

Table 3. Peak position of deconvoluted free ion and ion pair peak of SPE film based on (PEO–PVC)-LIPF$_6$ + x wt.% TiO_2 ($0 \leqslant x \leqslant 20$).

	Free ion		Ion pair		
Nanofiller (wt.%)	Peak (cm^{-1})	Area (%)	Peak (cm^{-1})	Area (%)	Correlation coff. (r^2)
0	835	47.06	847	52.93	0.987 199 80
3	836	47.32	847	52.47	0.990 810 45
7	846	50.90	846	50.90	0.984 540 13
10	835	48.20	847	51.79	0.995 124 52
15	835	49.02	847	50.97	0.978 545 70
20	836	47.71	847	52.28	0.990 922 05

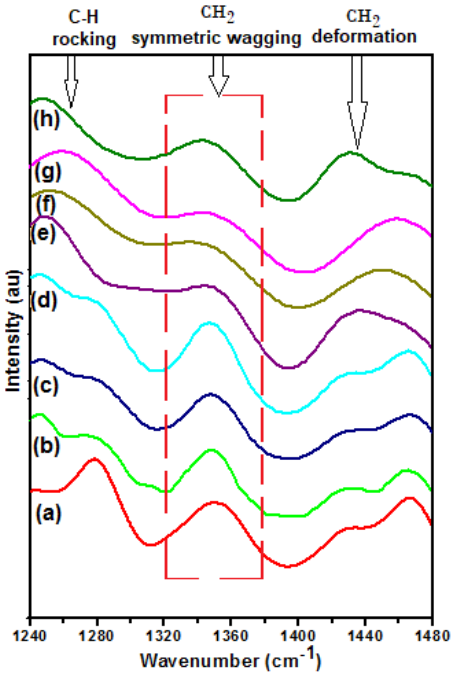

Figure 9. FTIR spectra of SPE films: (a) blend polymer and (PEO–PVC)-$LIPF_6$ + x wt.% TiO_2 films, (b) $x = 0$, (c) $x = 1$, (d) $x = 3$, (e) $x = 7$, (f) $x = 10$, (g) $x = 15$, (h) $x = 20$.

Another interesting IR frequency region is from 2800–3000 cm^{-1}, which corresponds to the symmetric and asymmetric stretching mode of CH_2. A single peak is observed in figure 10 and the presence of asymmetry confirms the presence of two peaks in this region. This is deconvoluted into two peaks at 2885 and 2910 cm^{-1}, as shown in figure 10. The former arises from the symmetric stretching ($\nu(CH_2)_s$) mode, and the latter is due to the asymmetric stretching ($\nu(CH_2)_a$) mode. However, band splitting is obtained (figure 10) into two bands, one near 2880 cm^{-1} and another near 2910 cm^{-1} corresponding to symmetric CH_2 stretching ($\nu(CH_2)_s$) and asymmetric CH_2 stretching ($\nu(CH_2)_a$), respectively. On the addition of salt, both symmetric and asymmetric stretching modes shift their position, indicating evidence of the interaction of salt with the polymer host.

The deconvolution of the peak is done to get the original peaks in a given wavenumber range by Voigt Amp fit. The symmetric and asymmetric stretching mode shifts to a lower wavenumber side from 2885 to 2883 cm^{-1} and 2910 to 2903 cm^{-1} on the addition of nanofiller in the PS complex, respectively. The addition of nanofiller affects the symmetric/asymmetric mode, as observed in terms of change in the peak area and it may be due to the interaction of a surface group of nanofillers with the polymer host. This shift in band position shows the effect of nanofiller on the interaction between polymer-salt, and polymer-salt-nanofiller in SPEs. The FTIR spectrum provides direct evidence of interaction (polymer–ion-nanofiller interaction) in SPE films. Generally, these interactions impact strongly the dissociation of salt, which results in more free ions and results in faster ion dynamics. Also, at higher nanofiller content, upward shift in wavenumber is shown by asymmetric mode (2914 → 2910 → 2909 → 2903 cm^{-1}), which provides evidence of chain stiffening. This is further studied in the following section and is correlated with electrical properties.

3.4. DSC analysis

DSC was implemented for confirming the increase of electrical conductivity, which is due to the increase of free ions and decrease of crystallinity. Figures 11(I) and (II) show the DSC results for SPEs with different nanofiller content. The endothermic peak observed at high temperature is attributed to the melting point of SPE. The percentage of crystallinity (X_c) was calculated as $X_c = \frac{\Delta H_m}{\Delta H_m^o} \times 100$ where ΔH_m is the melting enthalpy obtained from the DSC measurement and ΔH_m^o is the melting enthalpy of pure 100% crystalline PEO (188 J g^{-1}) [59]. The melting peak of the polymer blend PEO–PVC was observed at 79 °C and shifts towards a lower temperature of 69 °C on the addition of the salt (figure 11(I)). Also, the area under the peak decreases, which depicts the decrease of crystallinity in the polymer electrolyte. As polymer crystallinity is hindered due to the coordinating interaction of the polymer chain with cation. This lowering of the melting temperature and melting peak area is strong evidence of enhanced amorphous content. Further, the enthalpy of melting and melting temperature follows the same trend with the addition of the nanofiller at lower content and this type of trend evidences the increased polymer chain flexibility and ion mobility [60]. The area under the melting curve was used to calculate the degree of crystallinity, and the glass transition temperature along with the melting temperature of SPEs are summarized in table 4. It may be concluded that the addition of nanofiller decreases the crystallinity and is due to surface interaction provided by the nanofiller with the polymer host and lithium salt.

Now, in figure 11(II) the slight downward transition in the thermal curve with the mid-point in the range −30 to −60 °C reflects the glass transition temperature (T_g) of SPEs and shows a reduction with the addition of the salt. Furthermore, the addition of the nanofiller demonstrates a left shift on the x-axis and suggests the increase in conductivity due to the increase of polymer flexibility (table 4). Nanofiller with high surface area weakens the interaction of cation with the ether group and supports the fast ion migration via the additional conducting pathways provided by the nanofiller surface. The T_g corresponding to PVC is not observed, and it may be due to overlapping of the peak with the melting peak of PEO. So, the presence of single glass transition temperature and a shift in glass transition temperature of PEO for polymer blends confirms better miscibility of both polymers [61, 62]. The polymer miscibility is due to the presence of strong intermolecular interactions such as hydrogen bonding, between the chlorine atoms of PVC with PEO, having non-bonded electrons, such as oxygen. The presence of strong interaction reduces the Gibbs free energy, which is an indication of the homogenous mixing of polymers [63, 64]. The next section further correlates the DSC parameters with electrical properties.

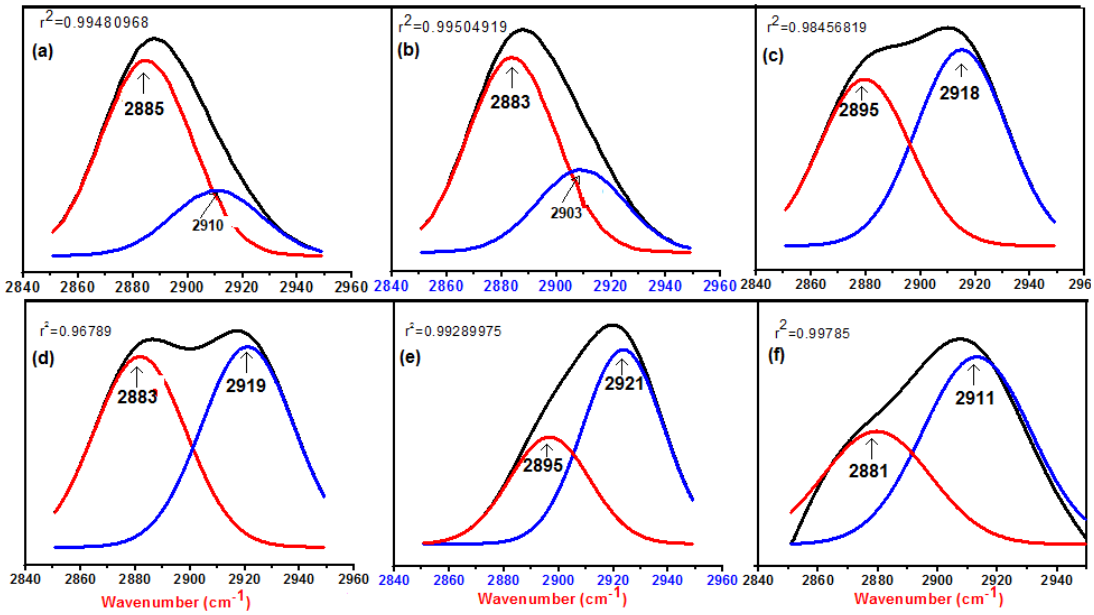

Figure 10. Variation in symmetric and asymmetric stretching mode (PEO–PVC)-LIPF$_6$ + x wt.% TiO_2 films: (a) $x = 0$, (b) $x = 3$, (c) $x = 7$, (d) $x = 10$, (e) $x = 15$, (f) $x = 20$.

3.5. Complex impedance spectroscopy (CIS) analysis

CIS is a powerful tool for investigating the electrical properties of materials and motion of bound/mobile ion charges in the solid or liquid materials using a small signal (~50 mV) in the frequency domain from 1 Hz–1 MHz. The principle of impedance spectroscopy is based on the ability of a medium to pass an alternating electrical current. When an alternating electric field is applied across the sample, dipole interaction with the corresponding ions due to the Coulomb electric force leads to rearrangement, depending on the mobility of backbone (Li^+) [53]. The experimental impedance response, when fitted using the non-linear least squares (NLS) model by means of a computer program (Z_{Simp}Win), agrees well with the corresponding theoretical pattern, suggesting validity of the experimental results, and an equivalent circuit is proposed to interpret the complex impedance spectra.

Figures 12(a)–(h) represent the complex impedance plot of prepared SPE films at different nanofiller concentration. For polymer blend, a semicircle curve is obtained with a diameter R_b extending along the real axis from the origin, as in figure 12(a). Figure 12(b) shows typical complex impedance spectra of the blend polymer salt complex. It is usually true that high-frequency response conveys information about properties of an electrolyte such as bulk resistance/long range ordering (due to the migration of ions). The low-frequency response carries information about the electrode/electrolyte interface. The effect of nanofiller addition into the blend polymer salt complex matrix appears to modulate the electrical behavior of the composite matrix. This change is designated by the changing pattern of the complex impedance spectrum with various nanofiller concentrations. The value of bulk resistance decreases with the addition of salt compared to the polymer blend and further addition of nanofiller decreases the bulk resistance. At low frequencies, there is sufficient time to accumulate the space charge across the electrode–electrolyte interface and that results in an enormous increase in the measured double-layer capacitance [65, 66]. A modification such as a semicircular arc at high-frequency and a low-frequency steep spike in the impedance spectrum of the SPE films suggests a drastic change in the electrochemical properties of the PS film on the addition of nanofiller. The high-frequency semicircular arc at high frequency in the polymer blend is attributed to the contribution due to the presence of resistance and capacitance in the bulk material of the sample. The absence of the semi-circular portion (figures 12(b)–(h)) may be attributed to the fact that the corresponding characteristic frequency is higher than the frequency of 1 MHz. The presence of a steep spike (non-vertical) at an angle of less than 90° to the real axis in the low-frequency region suggests the formation of space charge at the electrode–electrolyte interface region, commonly referred to as the double-layer capacitive effect due to a non-faradic process occurring at the interface of the SPE films and SS electrode [13, 67–69]. It also indicates the inhomogeneous nature of the electrode–electrolyte interface. This type of behavior suggests that migration of ions occurs via free volume available in the polymer matrix and can be represented by a resistor [70, 71]. The low-frequency response of the CIS pattern remains almost identical for the SPE films, as in the case of PS film irrespective of nanofiller variation. This represents the accumulation of space charge carriers at the interface of the ionically conducting SPE films and SS blocking electrode. The disappearance of the semicircular region in the impedance spectra after the addition of nanofiller leads to the conclusion that the total conductivity is due to the conduction of fast ion charge migration, so only a diffusion process takes place [72–75]. This also indicates that conduction is now supported by dispersed nanofiller with the surface group.

The experimental impedance response, was fitted using the NLS model by means of a computer program (Z_{Simp}Win).

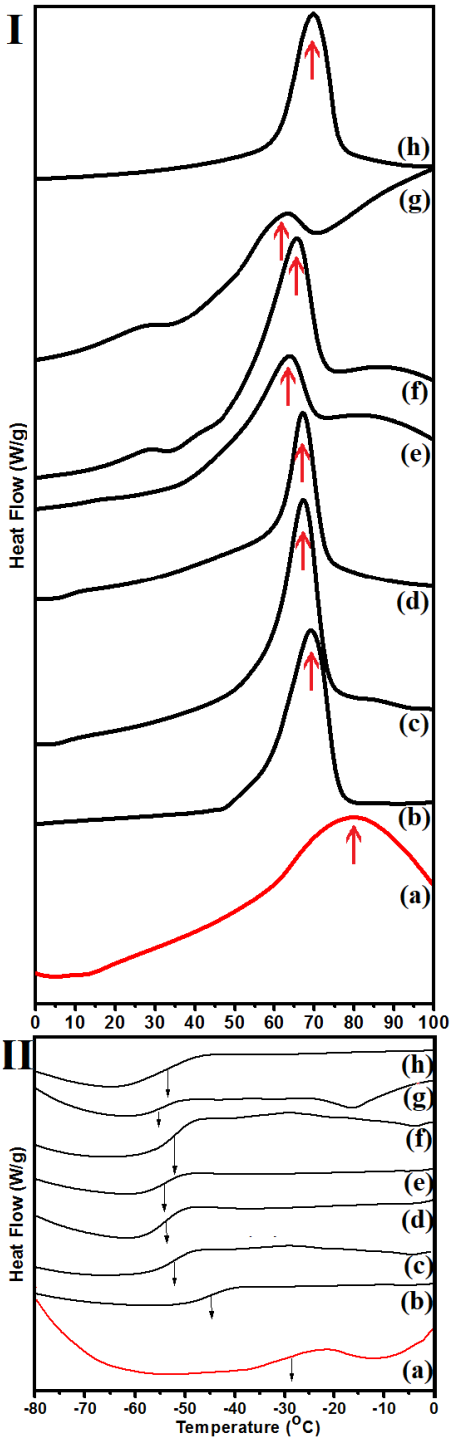

Figure 11. DSC curve (I) melting peak, (II) glass transition temperature for various SPEs for films: (a) host blend polymer and (PEO–PVC)-$LIPF_6$ + x wt.% TiO_2 films, (b) $x = 0$, (c) $x = 1$, (d) $x = 3$, (e) $x = 7$, (f) $x = 10$, (g) $x = 15$, (h) $x = 20$.

An electrical equivalent circuit model of the sample impedance response appears to be consistent with a fit containing two parallel combinations of constant phase element (CPE) and a resistance connected in series with each other. The presence of a CPE in the material sample is evidence of its multiphase character encompassing both crystalline and amorphous microstructure and a mixture of the two phases in the PS complex film and $Z_{CPE} = \frac{1}{Q_o(jw)^n}$, where Q_o and n are

Table 4. Glass transition temperature (T_g), melting temperature (T_m), enthalpy of melting and degree of crystallinity for polymer blend, polymer salt, and x wt.% ($x = 0$, 1, 3, 7, 10, 15, 20) nanofiller-added SPEs.

Polymer electrolyte	T_g (°C)	T_m (°C)	ΔH_m (J g^{-1})	X_c (%)
PEO–PVC blend	−30	78	174.8	92.97
0	−45	69	110.2	58.61
1	−52	67	78.42	41.71
3	−53	67	66.28	29.93
7	−53	63	36.48	19.40
10	−52	65	51.56	27.42
15	−56	63	21.37	11.36
20	−54	69	42.7	22.71

fitting parameters and $n = 0$, 0.5, 1, and −1 for pure resistor, Warburg component, pure capacitor, and pure inductive component, respectively. From the fitting pattern of CIS (figure 12), it is clearly visible that the theoretical and experimental pattern are in good agreement with each other. Change in fitting parameters with filler concentration shows change in electrical properties [76–78].

The parameters recorded in table 5 are just to provide evidence for a change in the sample electrical response to a change in nanofiller concentration in the SPE films. The model of the electrical equivalent circuit remains identical in the pattern for the SPE and PS films with a vital difference in the values of bulk resistance (R_b), CPE Q_1 and Q_2 and their exponents n_1 and n_2, respectively. A high double-layer capacitance (C_{dl}) value in the SPE film with nanofiller (53.1 μF) compared to polymer salt (0.18 μF) film may be attributed to more dissociation of lithium salt due to the surface interaction of nanofiller with salt and the production of a greater number of charge carriers for conduction, which is in agreement with the deconvolution of FTIR.

3.5.1. Electrical conductivity analysis. To investigate the effect of nanofiller on polymer blend, different content of nanofiller were added to prepare the electrolyte. So, for electrical conductivity measurements using two blocking electrodes comprising SS|SPE|SS, equation (1) is used. The ionic conductivity of the polymer blend was 3.3×10^{-8} S cm^{-1}. The electrical conductivity increases with the addition of salt due to the availability of ions for migration and is a common feature of polymer electrolytes. Initially, at low nanofiller content, there is a small increase in conductivity value, but with the addition of nanofiller the increase is due to the release of more free ions via interaction of the nanofiller-polymer-ion. Furthermore, the addition of nanofiller enhances the salt dissociation and a continuous increase can be seen [79]. The maximum value of conductivity was obtained for 7 wt.% nanofiller (~5×10^{-5} S cm^{-1}), which was three orders higher than the polymer blend and attributed to the complete dissociation of salt in the system, as evidenced by the FTIR spectra. Also, the maximum conductivity value may be correlated with the structure of the SPEs including the uniform distribution of the nanofiller in the polymer salt matrix, as can be seen

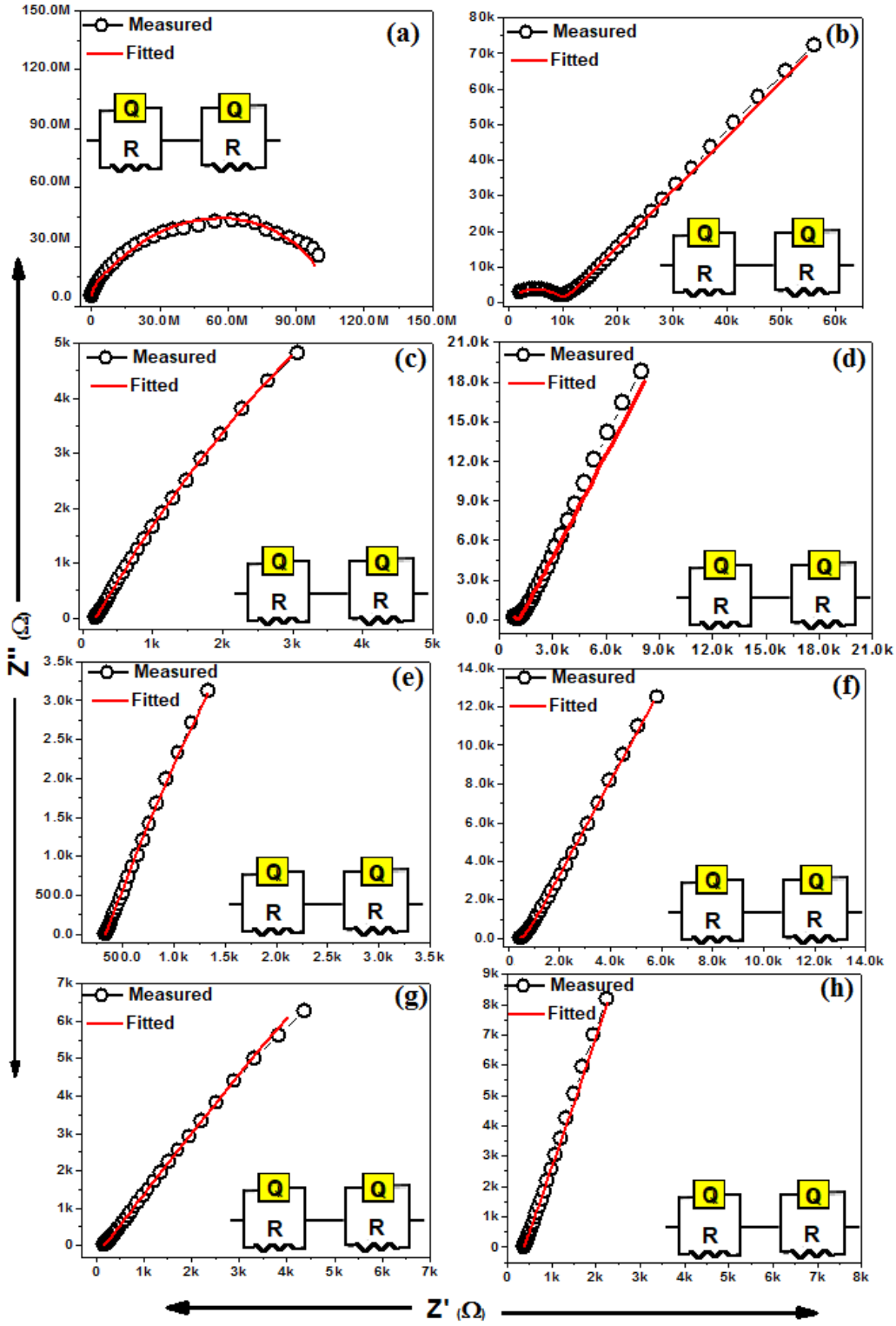

Figure 12. Nyquist plot of SPE films: (a) host blend polymer and (PEO–PVC)-LIPF$_6$ + x wt.% TiO_2 films, (b) $x = 0$, (c) $x = 1$, (d) $x = 3$, (e) $x = 7$, (f) $x = 10$, (g) $x = 15$, (h) $x = 20$.

by the FESEM and EDS mapping. The addition of nanofiller also makes the polymer chain flexible, which results in fast segmental motion and an increase in conductivity is observed. The characteristic conductivity variation with different nanofiller agrees well with the nanofiller-dependent changes in the fraction of the free anion in the SPE system. Furthermore, to support the investigated results, the correlation of various critical parameters of electrical transport was done, and a model is proposed in a later section.

3.6. Dielectric spectroscopy analysis

3.6.1. Complex permittivity analysis. Dielectric analysis of SPE materials is desirable to investigate in detail the transport

Table 5. Fitted parameters of NLS fit of the samples consisting of SPE films (PEO-PVC)-$LIPF_6$ + x wt.% TiO_2 ($0 \leqslant x \leqslant 20$).

Sample name (x wt.% TiO_2)	Q_1	n_1	Q_2	n_2	C_{dl} (μF)
PEO–PVC blend	3.5×10^{-4}	0.052	5.42×10^{-5}	0.67	0.10
$x = 0$	1.5×10^{-3}	0.035	2.18×10^{-5}	0.66	0.18
$x = 1$	4.3×10^{-4}	0.018	4.31×10^{-5}	0.74	9.21
$x = 3$	2.72×10^{-5}	0.015	3.79×10^{-7}	0.82	21.1
$x = 7$	2.8×10^{-3}	0.002	6.57×10^{-5}	0.8	53.1
$x = 10$	1.73×10^{-5}	0.045	1.86×10^{-5}	0.76	11.9
$x = 15$	4.3×10^{-3}	0.025	3.97×10^{-5}	0.8	25
$x = 20$	1.79×10^{-5}	0.037	2.74×10^{-3}	0.72	11

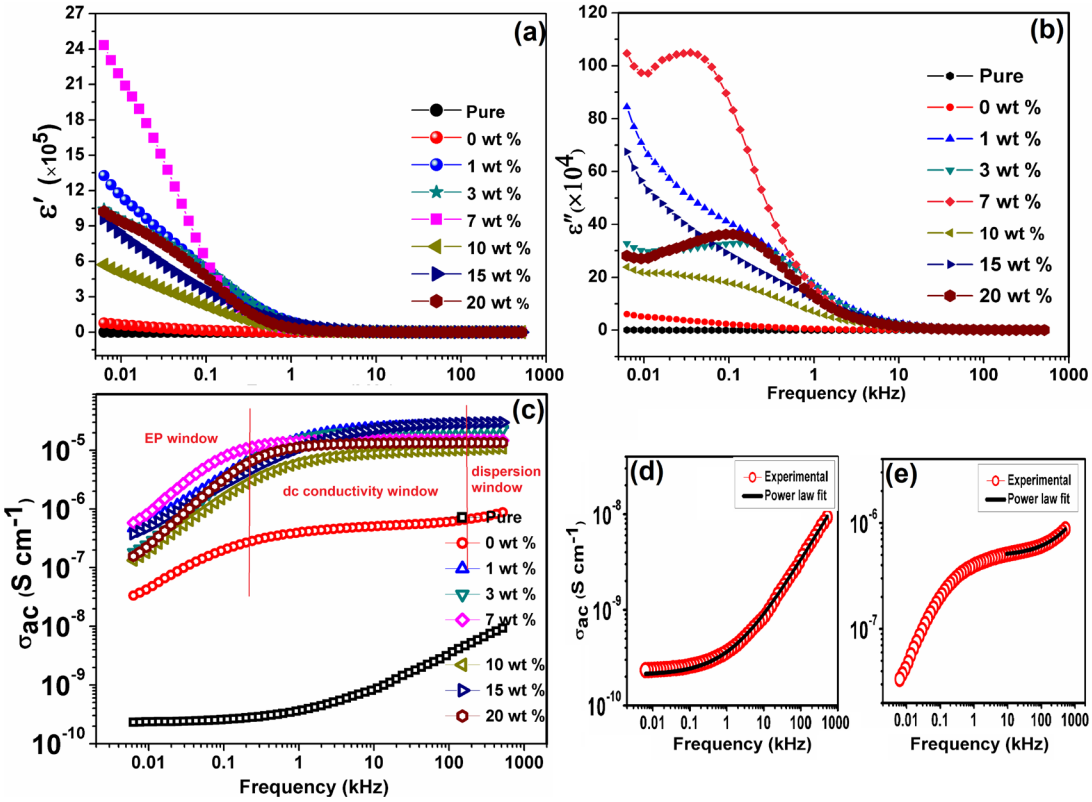

Figure 13. Variation of (a) real (ε'), (b) imaginary part (ε'') of dielectric constant, (c) AC conductivity against the frequency for: (a) PEO–PVC, PEO–PVC + $LIPF_6$ − x wt.% TiO_2 films, (b) $x = 0$, (c) $x = 1$, (d) $x = 3$, (e) $x = 7$, (f) $x = 10$, (g) $x = 15$, (h) $x = 20$. (d), (e) JPL fit of AC conductivity at high frequency for polymer blend and polymer salt system.

of ions and is explained in terms of the real and imaginary parts of complex permittivity (ε^*). The dielectric permittivity describes the polarizing ability of material in the presence of an applied external electric field. As permittivity is a function of frequency, it is a complex quantity, as shown below:

$$\varepsilon^* = \varepsilon' - j\varepsilon''. \tag{5}$$

The real part of dielectric permittivity (ε') is proportional to the capacitance and measures the alignment of dipoles, whereas the imaginary part of dielectric permittivity (ε'') is proportional to conductance and represents the energy required to align the dipoles. Here, ε' is related to the stored energy within the medium and ε'' to the dielectric energy loss of energy within the medium. The real (ε') and imaginary (ε'') parts of the dielectric permittivity are evaluated using the impedance data by equations (6) and (7):

$$\varepsilon' = \frac{-Z''}{\omega C_o \left(Z'^2 + Z''^2\right)}, \tag{6}$$

$$\varepsilon'' = \frac{Z'}{\omega C_o \left(Z'^2 + Z''^2\right)}, \tag{7}$$

where C_o ($=\varepsilon_r \cdot A\ t^{-1}$) is the vacuum capacitance, ε_r is the permittivity of free space and ω is the angular frequency.

Figures 13(a) and (b) show the recorded dielectric constant (ε') and dielectric loss (ε'') as a function of frequency with different nanofiller. From the plot, it can be seen that ε' decreases with the increase of frequency for all the systems and reaches the steady state near 10 kHz for all samples. Moreover, both values are higher at low frequency and decrease with the increase in frequency, and that indicates polarization effects due to charge carriers near the electrodes and also due to the dipoles, which

do not begin to follow the field variation at higher frequencies [80–84]. The incorporation of nanofiller increases the dielectric constant, since the growth of a number of charge carriers occurs and enhanced ion mobility is achieved. The dielectric constant is higher for 7 wt.% nanofiller content, which is in close agreement with conductivity data and supports the present investigation of fast SSIC. The low-frequency response is coined as the electrode polarization (EP) effect, which is due to the formation of electric double-layer capacitances due to free charge build-up at the electrolyte/electrode interface. Meanwhile, the higher-frequency region restricts dipoles contributing to EP due to insufficient response time on the application of electric field, and dielectric constant decreases (ε'). Figure 13(b) shows the tremendous value of dielectric loss (ε'') towards the low-frequency region and may be attributed to the accumulation of free charge carrier at the electrode/electrolyte interface because in this region charge carriers get sufficient time to accumulate at the electrode/electrolyte interface and contribute to the large dielectric loss.

3.6.2. AC conductivity analysis. The AC electrical measurements (AC conductivity) of PEO–PVC-based SPE were obtained at a frequency range from 1 Hz–1 MHz at room temperature. The frequency variation of the real part of conductivity is shown in figure 13(c). The standard feature indicates that AC conductivity increases with increasing the applied frequency due to fast ion migration, which may be attributed to the increased number of mobile charge carriers and results in charge-up build or EP. The frequency-dependent real part of conductivity shows three distinct regions: (i) low-frequency dispersion region, (ii) frequency-independent plateau region and (iii) high-frequency dispersive region. The low conductivity value at the low-frequency dispersion region is the result of the accumulation of ions (EP) due to the slow periodic reversal of the electric field. The intermediate region at slightly higher frequency corresponds to the frequency-independent plateau region, and DC conductivity can be evaluated from here. At the high-frequency window, the region is due to short-range ion transport associated with AC conductivity. The polymer blend and polymer salt system show all the three regions, but the low-frequency region disappears with the addition of salt and nanofiller. All the systems show a shift in both the intermediate-frequency region and high-frequency region towards a high-frequency window. The DC conduction is attributed to random hopping of ions between localized states, while the cause of AC conduction is correlated ion hopping in high-frequency regions. For all nanofiller and dispersed polymer electrolytes (figure 13(c)), the high-frequency dispersion region corresponds to bulk relaxation phenomena and falls outside the measured frequency range, and hence, could not be observed. This observation is indicative of the complex transport process possibly due to the combined effect of space charge polarization (EP at the electrode–electrolyte interface) at low frequency followed by long-range ion migration at high frequency [81]. AC conductivity is evaluated by equation (8):

$$\sigma_{ac} = \omega \varepsilon_o \varepsilon'', \tag{8}$$

where ω is the angular frequency, ε_o is the dielectric permittivity of the free space and ε'' represents the dielectric loss.

The conductivity of the polymer blend is very low, as observed in figure 13(c) and is due to the EP effect causing a decrease in a number of free charge carriers. The addition of salt shifts the curve towards the high-frequency region, which is evidenced by an increase in conductivity. The EP contribution to conductivity is clearly observed followed by the high dispersive effect, which is typical of a fast ion conductor and saturation limit of the EP effect, and is evidence of change in the mechanism of ion migration. The high-frequency dispersive region observed in the polymer blend and polymer salt system follows the universal Jonscher's power-law (JPL) response given by $\sigma' = \sigma_{dc} + A\omega^n$, where σ' and σ_{dc} are the AC and DC conductivities of electrolyte, while A and n are the frequency-independent Arrhenius constant and the power-law exponent, respectively. Basically, ion migration at low frequency results in a long relaxation time, and ion contribution can be seen in DC conductivity. The low chi-squared value of the order of 10^{-13} suggests the best JPL fit for the experimental results, and the fitted values are shown in the insets (figures 13(d) and (e)). The frequency-dependent region fitting provides an estimate of the pre-exponential factor (A) and fractional exponent (n). The value of n between 0.5 and 1 suggests that the SPE system is a true ionic conductor. The power-law behavior is a universal property of the materials.

3.7. Transference number analysis

The transference number of an ion in SPE is the fraction of the total current carried by the respective ion across a given medium. As different ions have different mobility, they may bring drastically different portions of the total current [85]. The total active ionic transference number of SPEs has been studied by separation of the ion and electronic contribution. The variation of current as a function of time for the PS film and SPE films with varying nanofiller concentration (x wt.% TiO_2; $0 \leqslant x \leqslant 20$) at room temperature is recorded, as shown in figure 14.

The current decays immediately and asymptotically approaches the steady state. The pattern shows two currents; one is the initial current, total current (i_t) and after that, there is a sharp drop in the value of the current with the passage of time. After some time, the current reaches saturated value and the same trend of constant current is obtained for all the samples. The two processes of migration of ions under the influence of an external field and diffusion due to concentration gradients are hostile, and therefore after a sufficiently long time, the establishment of the steady state is reached [17]. Initially, in the SPE membrane high current is attributed to the migration of both electrons and ions, while current after cell polarization due to blocking electrodes (SS) is attributed to the movement of electrons only, known as the residual electronic current (i_e). The initial decrease in current until the saturation state is primarily due to the formation of the passivation layer on the electrodes. Now, the concentration gradient of ions develops

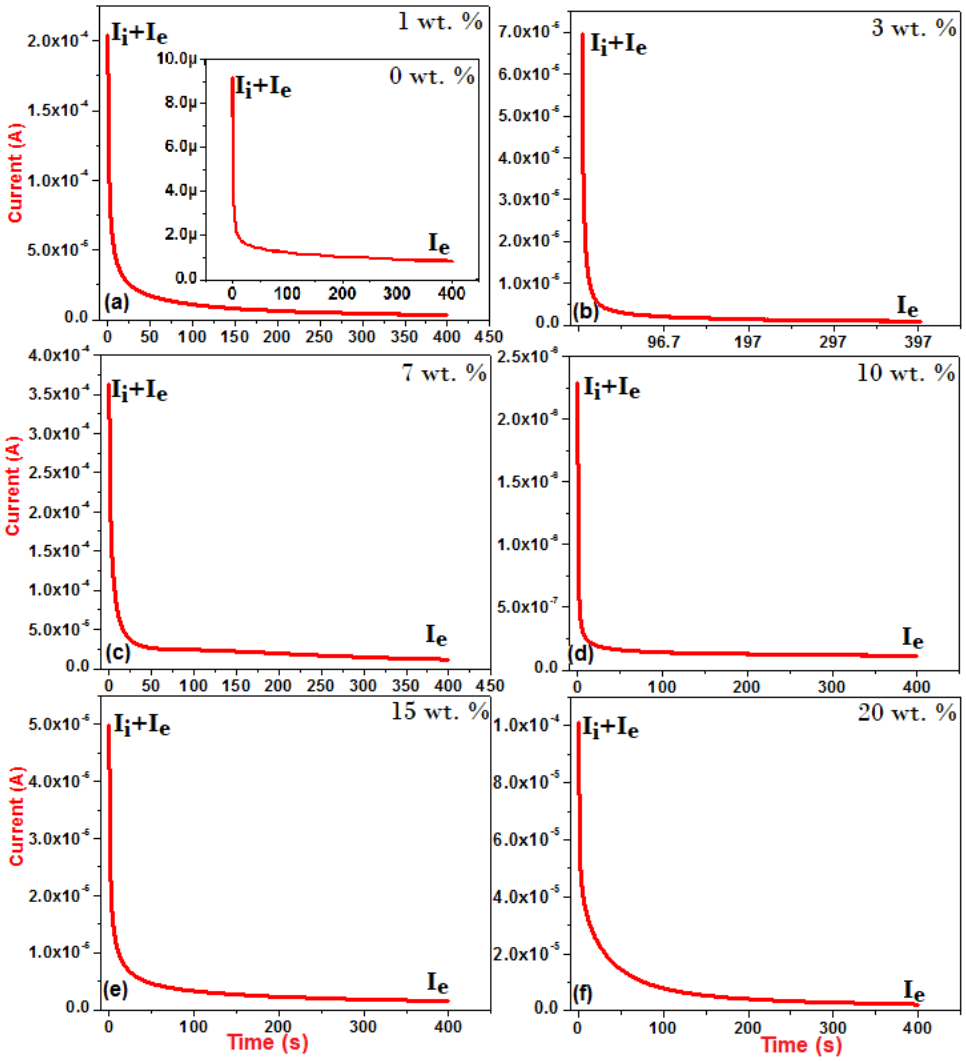

Figure 14. Ion transference number of SPE films (PEO–PVC)-$LIPF_6$ + x wt.% TiO_2 films: (a) $x = 1$, (b) $x = 3$, (c) $x = 7$, (d) $x = 10$, (e) $x = 15$, (f) $x = 20$ ($x = 0$ wt.% in inset).

Table 6. Different contributions of electrical conductivity and transport number for (PEO–PVC)-$LIPF_6$ + x wt.% TiO_2 ($0 \leqslant x \leqslant 20$).

Sample name (x wt.% TiO_2)	Transference number	Electrical conductivity (S cm^{-1})	Electronic conductivity (S cm^{-1})	Ionic conductivity (S cm^{-1})
PEO–PVC blend	0.67	3.33×10^{-8}	1.09×10^{-8}	2.23×10^{-8}
$x = 0$	0.90	0.51×10^{-6}	5×10^{-10}	0.45×10^{-6}
$x = 1$	0.99	1.84×10^{-5}	1.8×10^{-10}	1.82×10^{-5}
$x = 3$	0.98	4.37×10^{-5}	8.7×10^{-10}	4.28×10^{-5}
$x = 7$	0.96	4.99×10^{-5}	1.99×10^{-9}	4.89×10^{-5}
$x = 10$	0.95	2.08×10^{-5}	1.04×10^{-9}	1.97×10^{-5}
$x = 15$	0.97	4.87×10^{-5}	1.46×10^{-9}	4.72×10^{-5}
$x = 20$	0.98	3.58×10^{-5}	7.1×10^{-10}	3.50×10^{-5}

and opposes the applied current by diffusion of ions. As the polarization builds up because of the applied voltage, the ions were blocked at the blocking electrode, thereby preventing the ionic current (i_{ion}), and the last current comprises only the electronic current (i_e) [86]. The high value of the transference number also indicates a reduction in concentration polarization. This improves the ionic transport, and after a long time, the presence of the steady state evidences the current flow only due to the migration of Li^+ cations in the electrolyte and anion movement has entirely ceased [87, 88].

The estimated value of the ionic transport number (t_{ion}) using the experimental data of i_t and i_e is obtained with equation (2) and given in table 6. Further ionic and electronic conductivity contribution is estimated using equations (9)–(11).

$$i_t = i_{ion} + i_{elec}\,. \tag{9}$$

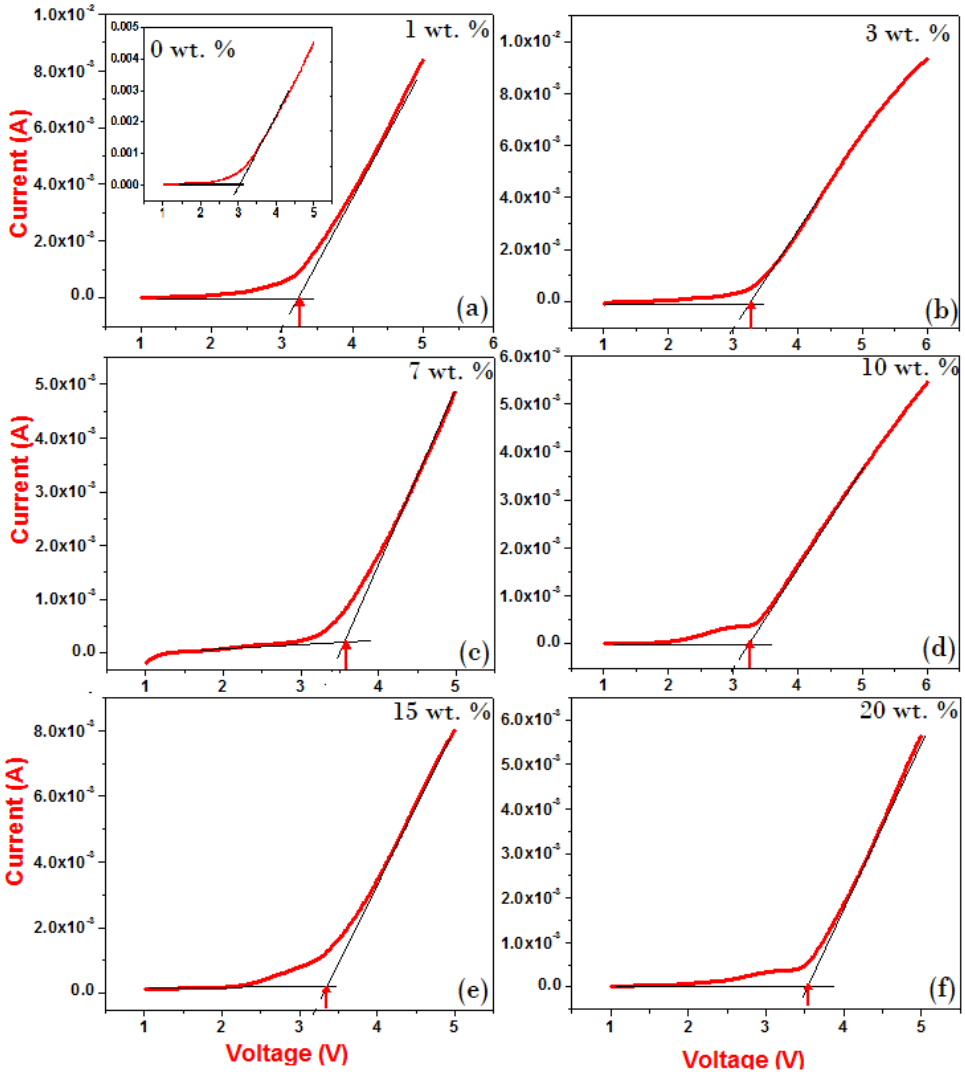

Figure 15. LSV of SPE films (PEO–PVC)-LIPF$_6$ + x wt.% TiO_2 films: (a) $x = 1$, (b) $x = 3$, (c) $x = 7$, (d) $x = 10$, (e) $x = 15$, (f) $x = 20$ ($x = 0$ wt.% in inset).

Therefore,

$$\sigma_{\text{ionic}} = \sigma_{\text{electrical}} \times t_{\text{ion}} \tag{10}$$

$$\sigma_{\text{electronic}} = \sigma_{\text{electrical}} \times t_{\text{electronic}}. \tag{11}$$

The transference number values clearly indicate that the SPE samples are a chiefly ionic conductor with $t_{\text{ion}} \approx 0.99$ and negligible electronic contribution and is sufficient to fulfill the requirement of solid-state electrochemical cells [89, 90]. The ionic conductivity and electronic conductivity are also in absolute correlation with the electrical conductivity value. Beside this, the electronic conductivity is almost within the desired limit ($\leqslant 10^{-7}$ S cm^{-1}) for its utilization in energy-storage devices.

3.8. Electrochemical stability window

A wide electrochemical stability window of the electrolyte is an important parameter for the effective performance of energy-storage/conversion devices. The working voltage or electrochemical stability window of the SPE membranes has been studied by observing the variation of current and voltage (I and V) using the LSV technique (figure 15) for PS films and SPE films with nanofiller. Initially, there is almost constant current through the electrodes up to 2 V, while after that with an increase of the voltage there is a slow increase in current followed by an abrupt change corresponding to the onset of the decomposition process of the electrolyte. This small current up to 2 V might be attributed to the change of the SS surface. This kind of behavior is different from both PS and SPE films and provides direct evidence of enhancement in the working voltage or electrochemical stability window after the addition of nanofiller compared to PS films. The voltage value is obtained by extrapolating the higher-voltage linear current with the x-axis. During the LSV, the working electrode is polarized, and the onset of the current may be taken as the decomposition voltage of the given polymer electrolyte [91]. The addition of nanofiller in PS films gives a safe operating range with the majority of the lithium battery electrode couples [7]. A comparison of this with PS films indicates an enhancement in the voltage window in SPE films (2.8– ~3.5 V) with a maximum value of ~3.5 V. Of course, the voltage

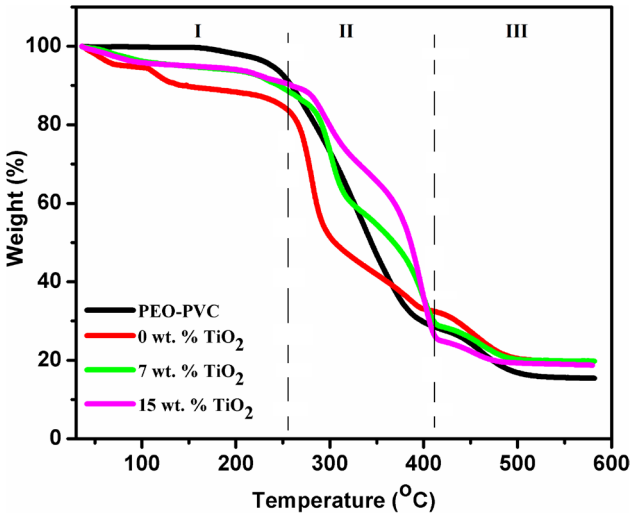

Figure 16. TGA curves of PEO–PVC blend, 0 wt.% TiO_2, 7 wt.% TiO_2 and 15 wt.% TiO_2.

stability window enhancement appears to be a function of the wt.% of nanofiller evident from the results.

3.9. TGA

Now, the thermal stability of the prepared polymer nanocomposite films is investigated by TGA. As during the operation of a battery device, especially in electric vehicles, high temperature may be reached, which may decompose the constituents of the polymer electrolyte and may lead to an explosion [92]. So, it becomes the principal responsibility to investigate the thermal stability of the materials used in the system. Figure 16 represents the thermo-grams of the PEO–PVC blend and PEO–PVC + $LiPF_6$ with 0 wt.% TiO_2, 7 wt.% TiO_2 and 15 wt.% TiO_2. For better insight, the thermo-gram is divided into three regions, depending on the weight loss.

In *region* 1, initially, a small weight loss is observed and that may be due to the evaporation of the solvent present in the skeleton of the films. The PEO–PVC blend with salt shows a reduction in thermal stability compared to the PEO–PVC blend and it may be due to more aprotic solvent absorbed by the salt. Also, the coordinating interaction between the cation and ether group affects the thermal stability of the polymer salt complex. Meanwhile, the addition of nanofiller indicates a reduction of solvent content and better thermal stability is observed compared to the polymer salt system. As dispersion of nanofiller alters the interaction between the polymer chain and a cation, this leads to the creation of some new interaction between the nanofiller and cation, which affects the thermal stability. Now, in *region* 2, the PEO–PVC blend shows rapid weight loss (approximately 70%), while the addition of salt prevents the rapid loss and thermal stability is improved. This may be attributed to the cation coordination with the ether group of the polymer chains. This may be due to the breakage of weak interaction and then the materials start to decompose. Meanwhile, for the polymer salt system with nanofiller, the thermal stability curve shifts to the right side or thermal stability is improved. All films are thermally stable up to approximately 300 °C, which is considerable for application purposes. This multi-step process of weight loss indicates that the present system is the BPE. In *region* 3, the polymer matrix constituents start to degrade and weight loss is maximum. But, the SPE cannot be completely decomposed even when the temperature reaches 600 °C. All films display good thermal stability up to 300 °C, which is enough to fulfill the demand of the electrolyte in energy-storage/conversion devices.

3.10. Correlation of free ion area (%), C_{dl}, σ_{dc}, n, μ, D, T_g (°C), T_m (°C), ΔH_m (J g^{-1}) and X_c (%)

The electrical conductivity value of SPE films is directly linked with the number of free charge carriers and mobility, as in given equation (12):

$$\sigma = nq\mu, \tag{12}$$

where n is a fraction of free ion, q is an anionic charge, and μ is mobility of the ions. As q and μ are constant for a particular matrix, conductivity only depends on the number of free charge carriers, as studied in the following section [81]. An excellent correlation of maxima in a fraction of free ion, double-layer capacitance, and conductivity with nanofiller content is in support of our scheme (figures 17(a)–(c)). The increase in ionic conductivity may be attributed to the existence of an amorphous layer with nanofiller on a surface having a surface group, which provides channels for ion transport. The electrical conductivity calculated for different nanofiller content is plotted in figure 17(d). Double-layer capacitance is calculated using equation (13) and is shown in table 5. As nanofiller concentration increases, a number of free charge carriers are available for conduction, and this leads to an increase in capacitance value.

$$C_{\mathrm{dl}} = -\frac{1}{\omega z''}. \tag{13}$$

A comparison of conductivity values suggests an enhancement in conductivity after the addition of a small content of nanofiller of 1 wt.% in the polymer salt matrix. This may be attributed to the release of more free charge carriers due to polymer–ion-nanofiller interaction. The fraction of the free ions increases initially with the addition of even a small quantity of nanofiller and shows a maximum of ~7 wt.%, followed by a downward trend. Another maximum appears at ~15 wt.% of nanofiller particles, followed by a decreasing trend. This two maxima trends can be correlated with the fraction of free ions, double-layer capacitance, the number density of charge carriers, mobility and diffusion coefficients observed in the FTIR and impedance study discussed above. It may be noted that the variation of the fraction of ion pairs as a function of nanofiller concentration shows a minimum corresponding to each maximum in the free ions versus nanofiller content plots. Such variations of free and paired anions have been reported earlier in PMMA-based solvent-free polymer electrolyte composites [93].

The desirable property of a SPE is high ionic conductivity (σ), which is directly linked with number density (n), mobility

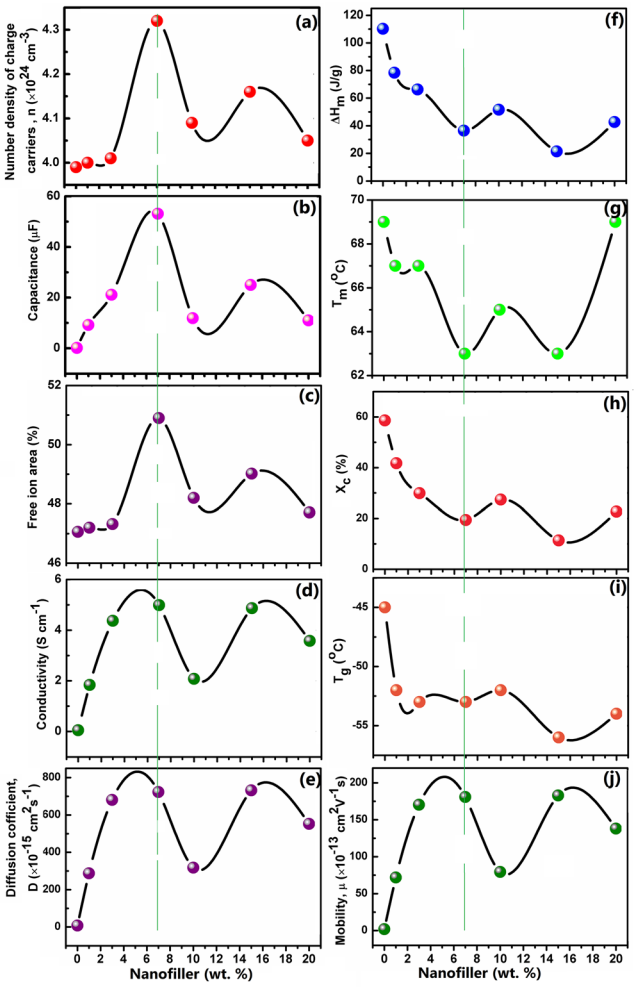

Figure 17. Plot of variation in: (a) charge carrier number density n, (b) double-layer capacitance C_{dl}, (c) free ions area (%), (d) DC conductivity σ, (e) diffusion coefficient D, (f) enthalpy of melting ΔH_m (J g^{-1}), (g) melting temperature T_m (°C), (h) crystallinity X_c (%), (i) glass transition temperature T_g (°C), and (j) charge carrier mobility (μ).

(μ) of charge carriers and diffusion coefficient (D) for any plastic separator, which stands for electrolyte cum separator. From conductivity analysis it is concluded that conductivity increases with the addition of salt in the polymer blend and the further addition of nanofiller leads to enhancement with two maxima, one at 7 wt.% followed by 15 wt.% and is due to the increase of mobility or number density of charge carriers. The mobility (μ) of ions indicates the degree of ease with which ions pass through media on the application of an external electrical field and the diffusivity (D) represents the ease with which ions pass through media under a concentration gradient. Both parameters depend on the number of free charges, as ion pair formation or association may reduce the above number and mobility. Impedance and FTIR study provides direct calculation of the number density of mobile ions and their mobility for performance and development of a good SPE. Here, the above parameters are calculated using the FTIR spectroscopy as proposed by Arof *et al* [94]. The variation in conductivity can be related to the number density (n), mobility (μ) and diffusion coefficient (D) of charge carriers in the electrolyte. FTIR deconvolution was done to determine the percentage area of free ion and ion pair and the areas are plotted as a function of various nanofiller (figure 8). The free ion area increases with the addition of nanofiller with the first maximum at 7 wt.% followed by another at 15 wt.%, as shown in figure 17(c). The number density (n), mobility (μ) and diffusion coefficient (D) of the mobile ions were calculated using equations (14)–(16):

$$n = \frac{M \times N_A}{V_{Total}} \times \text{free ion area } (\%) \tag{14}$$

$$\mu = \frac{\sigma}{ne} \tag{15}$$

$$D = \frac{\mu k_B T}{e}. \tag{16}$$

In equation (14), M is the number of moles of salt used in each electrolyte, N_A is Avogadro's number (6.02×10^{23} mol^{-1}), V_{Total} is the total volume of the SPE, and σ is DC conductivity. In equation (15), e is the electric charge (1.602×10^{-19} C), k_B is the Boltzmann constant (1.38×10^{-23} J K^{-1}) and T is the absolute temperature in equation (16). Table 7 lists the values of V_{Total}, free ions (%), n, μ, and D obtained using the FTIR method [94, 95]. It is observed that the ionic conductivity is closely related to the number density of mobile charge carriers, double-layer capacitance, mobility, and diffusion coefficient (figures 17(a), (e) and (j)). Figure 17 reveals the one-to-one correspondence between free ion area (%), ionic conductivity (σ), charge carrier number density (n), charge carrier mobility (μ) and diffusion coefficient (D). The thermal parameters T_g and T_m obtained from DSC analysis indicates that the addition of nanofiller suppresses the polymer chain recrystallization tendency, which directly confirms the increase of free volume or amorphous phase content at a lower temperature than polymer blend T_g and T_m (figures 17(h) and (i)). At very high nanofiller content, crystallinity shows a slight increase, which is due to the negligible effect of nanofiller on the polymer chain and may be attributed to the mutual interaction of nanofiller particles, which dominates the above the polymer–ion-nanofiller interaction. This result is also in good agreement with the associated FTIR ion–ion interaction and conductivity studies. The trend in variation in free ion area (%), conductivity, double-layer capacitance, n, μ and D, is almost identical. The above results are strongly in favor of desirable SPEs for energy-storage devices with the evidence provided by the FTIR and impedance analysis.

3.11. Self-proposed ion transport mechanism

The results and their analysis described above enable us to propose a model to explain the strong dependence of the ion conductivity of the polymer nanocomposite (PNC) films on nanofiller concentration. On the basis of the above data obtained by FTIR spectroscopy on polymer–ion-nanofiller interaction and excellent correlation with double-layer capacitance (C_{dl}), conductivity, number density (n), mobility (μ) and diffusion coefficient (D) have motivated us to analyze and propose a model, which

Table 7. Values of V_{Total}, free ions (%), n, μ, and D obtained using the FTIR method.

Nanofiller content (wt.%)	V_{Total} ($\times 10^{-1}$ cm^3)	Free ions area (%)	n ($\times 10^{24}$ cm^{-3})	μ ($\times 10^{-13}$ cm^2 V^{-1}s)	D ($\times 10^{-15}$ cm^2 s^{-1})
0	0.2	47.06	3.99	7.98	1.99
1	0.2	47.20	4.00	287.5	71.87
3	0.2	47.32	4.01	681.10	170.27
7	0.2	50.90	4.32	723.37	180.84
10	0.2	48.20	4.09	317.84	79.46
15	0.2	49.02	4.16	731.67	182.91
20	0.2	47.71	4.05	552.46	138.11

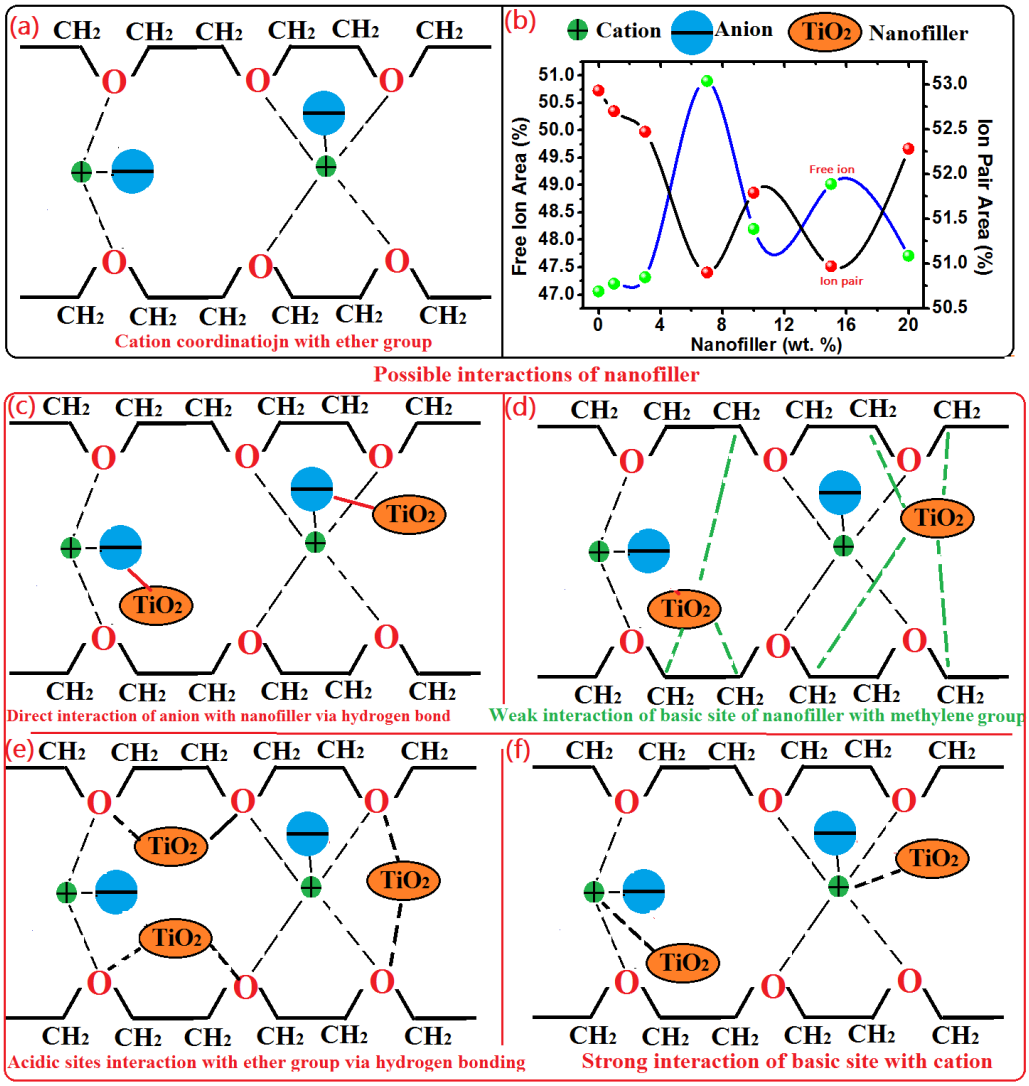

Figure 18. Various possible interactions between polymer–ion-nanofillers.

can provide better insight into the improvement of conductivity in the present study. Generally, when the lithium salt is added to the polymer electrolyte system, then the anion stays bound with the polymer chain while the cation gets coordinated with the ether group of the host polymer. This electron-rich group provides a path for ion migration in the polymer matrix. When the nanofiller is added in the polymer salt system, then there are two means by which it can affect the ionic transport or conductivity: (i) direct interaction of cation with nanofiller surface, (ii) interaction of nanofiller surface with a polymer chain. These lead to various possibilities for interaction: (i) cation coordination with the ether group (figure 18(a)), (ii) direct interaction of the anion with nanofiller via hydrogen bonding (figure 18(c)), (iii) weak interactions of basic site of nanofiller with the methylene group of polymer (figure 18(d)), (iv) acidic site interaction of nanofiller with the ether group via hydrogen bonding (figure 18(e)), (v) strong interactions of basic site of nanofiller with the cation (figure 18(f)).

Accordingly, in the present study, the first maximum observed at low nanofiller content is possibly due to the

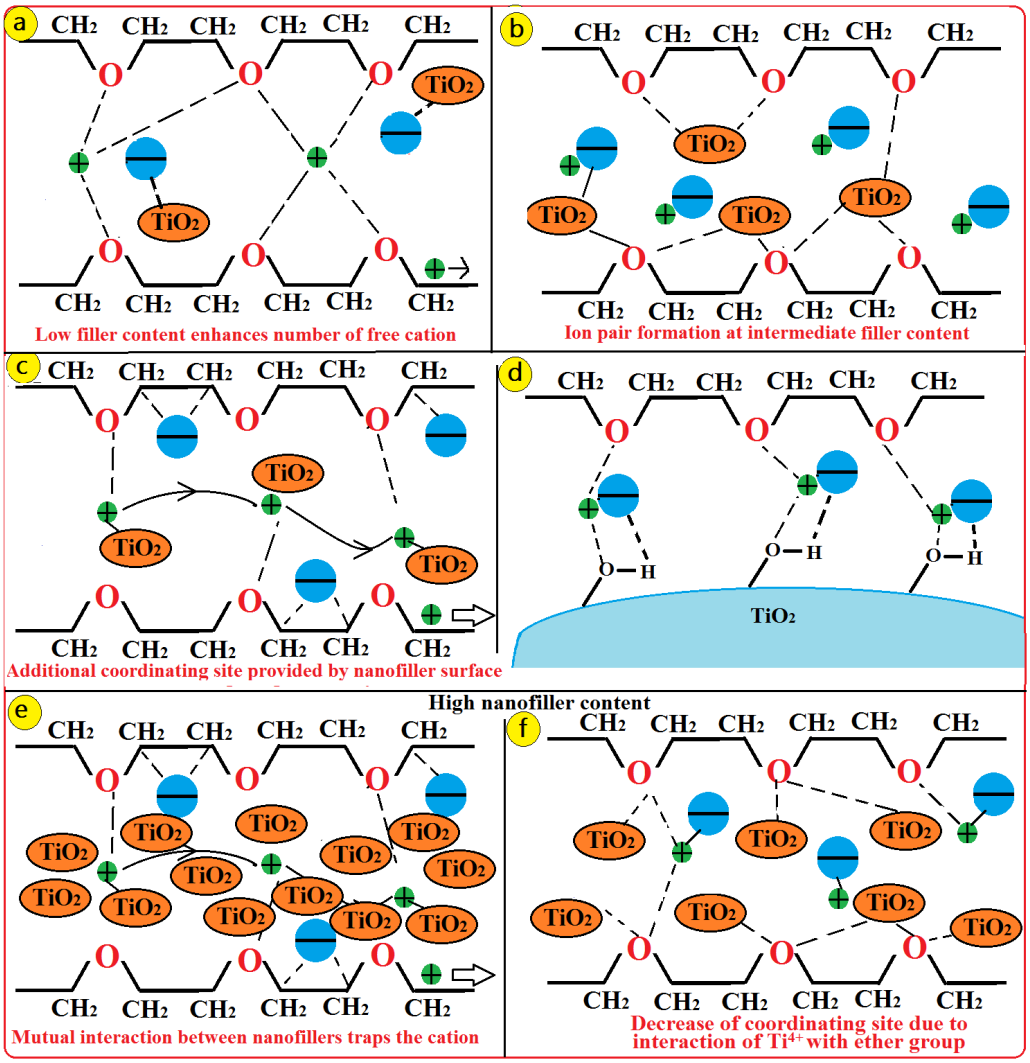

Figure 19. Pictorial model to illustrate the proposed ion conduction mechanism for the enhancement of ionic conductivity in SPEs on the basis of nanofiller content.

dissociation of free ions by nanofiller interaction with an anion via hydrogen bonding (figure 19(a)). The interaction between the anion and nanofiller dominates at lower nanofiller content and anions can be held on the nanofiller surface, and the cation easily migrates via the path provided by the polymer chain. The first maximum may also be linked to the formation of an additional space charge region between the polymer and nanofiller interface in the SPE due to the acidic nature of the TiO_2 nanofiller. Initially, the affinity for anions is more towards the nanofiller surface than the cation.

The acidic nature of nanofiller obstructs ion pairing due to the interaction of TiO_2 with PF_6^- ($TiO_2 + PF_6^- \leftrightarrow TiO_2$: PF_6^-) and a local electric field is formed, which assists in salt dissociation. As overall dielectric constant of the polymer matrix is also higher for the 7 wt.% nanofiller content and is most efficient for the conduction of lithium ions discussed above in dielectric analysis (figure 13(a)). Furthermore, the double-layer capacitance also followed the same trend as the conductivity maximum for the 7 wt.% nanofiller. This enhancement in conductivity also enhances the mobility and diffusion coefficient of the cation in the SPE system, as shown in figures 17(e) and (j). The decreasing trend in conductivity pattern for high nanofiller content is due to the increased ability of ion pairing, as nanofiller also interacts weakly with the ether group, and hence salt is not dissociated properly. This reduces the free ion charge carrier concentration, and conductivity enhancement is prohibited or there is a lowering of ion mobility (figure 17(j)). The reduction in conductivity value after the first maximum may be due to the formation of ion pairs (figure 19(d)) or the reduction of the double-layer capacitance, as evidenced by FTIR and impedance study (figures 17(b) and (c)). The second conductivity maximum observed may be due to the formation of the conductive path by the nanofiller grains, which promotes migration of the cation. The As –OH group on the nanofiller surface may play an effective role and interact with the anion via hydrogen bonding. It prevents the ion pairing, and free ions are produced, accompanied by an increase in conductivity or ion mobility (figures 19(c) and (d)).

At high nanofiller content, the decrease in conductivity after the second maximum may be due to two causes: (i) nanofiller aggregation, (ii) reduction of the suitable coordinating site, as represented in figures 19(e) and (f), respectively. The

former leads to localization of the cation and anion in the region of the cluster, which reduces the free ion for migration. Hence, conductivity decreases, as discussed in the FTIR spectra (figure 17(b)). The entrapment of ion in localized clusters may be due to the high surface area of nanofiller, and space charge layer leads to a blocking effect. Also, the presence of mutual interaction between the nanofiller surface may trap the cation and confine it in between the nanofiller aggregation region, and hence further forward movement of the cation is prevented. The immobile state achieved by the polymer chain decreases the conductivity due to termination of the conducting pathways for the ion migration and is in agreement with the mobility and free ion area (figures 17(c) and (j)). This does not support ion conduction. Also, at high nanofiller content, one possible reason may be a reduction of the coordinating site for lithium, which is due to the interaction of Ti^{4+} with the ether group of PEO, and hence a drop in conductivity is evidenced (figure 19(f)).

4. Conclusions

Free-standing SPE films based on (PEO–PVC)-$LiPF_6 + x$ wt.% TiO_2 have been prepared by the solution-cast technique. The XRD results reveal the occurrence of complexation between the polymer blend, salt and nanofiller. An FESEM micrograph provides evidence of change in the surface morphology and homogeneity with the addition of nanofiller; further EDS mapping confirms the uniform dispersion of nanofiller in the polymer salt matrix. The FTIR analysis confirmed the existence of polymer–ion, ion–ion, and polymer–ion-nanofiller interactions that improve the electrical transport properties. The FTIR results also indicate an increase in the fraction of free ions with the addition of nanofiller and are in good agreement with the plot of the conductivity, double-layer capacitance, mobility, and diffusion coefficient. The observed electrical conductivity is highest for 7 wt.% at about ~5×10^{-5} S cm^{-1} at room temperature and appears to be consistent with deconvolution of the FTIR results. TiO_2 nanofiller contributes to the conductivity enhancement in SPE through the formation of Lewis acid–base-type transient bonding and provides additional sites for Li^+ ion hopping. The variation in dielectric constant and AC conductivity provides an analysis of the dielectric property, and AC conductivity variation obeys the JPL. All SPEs exhibit good thermal stability up to 300 °C. DSC analysis shows a reduction in crystallinity with the addition of nanofiller and a decrease in glass transition temperature confirms faster segmental motion of the polymer chain or enhanced flexibility. The enhancement in ionic transference number and electrochemical potential window on the addition of nanofiller has been estimated. This improvement in electrical conductivity, potential window, ion transference number and mobility of SPE films suggests a prospective candidate for energy-storage devices such as lithium polymer batteries and solid-state polymeric supercapacitors. A self-proposed ion transport model for enhancement in conductivity has been reported to understand the role of nanofiller and is consistent with experimental data.

Acknowledgment

One of the authors gratefully acknowledges the financial support from CUPB and partial funding from the UGC Startup Grant (GP-41).

ORCID iDs

A L Sharma https://orcid.org/0000-0002-4630-8452

References

[1] Sharma A L, Shukla N and Thakur A K 2008 *J. Polym. Sci.* B **46** 2577
[2] Faraday M 1832 Experimental researches in electricity *Phil. Trans. R. Soc.* **122** 125
[3] Fenton D E, Parker J M and Wright P V 1973 *Polymer* **14** 589
[4] Armand M B 1986 *Annu. Rev. Mater. Sci.* **16** 245
[5] Sharma A L and Thakur A K 2011 *J. Mater. Sci.* **46** 1916
[6] Michael M S, Jacob M M, Prabaharan S R and Radhakrishna S 1997 *Solid State Ion.* **98** 167
[7] Sharma A L and Thakur A K 2013 *Ionics* **19** 795
[8] Gray F M 1997 *Polymer Electrolytes* (London: Royal Society of Chemistry)
[9] Bruce P G 1997 *Solid State Electrochemistry* vol 5 (Cambridge: Cambridge University Press)
[10] Murata K, Izuchi S and Yoshihisa Y 2000 *Electrochim. Acta* **45** 1501
[11] Choi B K, Kim Y W and Shin H K 2000 *Electrochim. Acta* **45** 1371
[12] Jacob M M, Prabaharan S R and Radhakrishna S 1997 *Solid State Ion.* **104** 267
[13] Fan L, Dang Z, Nan C W and Li M 2002 *Electrochim. Acta* **48** 205
[14] Joge P, Kanchan D K, Sharma P and Gondaliya N 2013 *Indian J. Pure Appl. Phys.* **51** 350
[15] Mohamed Ali T, Padmanathan N and Selladurai S 2015 *Ionics* **21** 829
[16] Premalatha M, Vijaya N, Selvasekarapandian S and Selvalakshmi S 2016 *Ionics* **22** 1299
[17] Prasanna C M S and Suthanthiraraj S A 2016 *Ionics* **22** 389
[18] Kumar K N, Kang M, Sivaiah K, Ravi M and Ratnakaram Y C 2015 *Ionics* **22** 815
[19] Ramesh S, Ramesh K and Arof A K 2013 *Int. J. Electrochem. Sci.* **8** 8348
[20] Reddeppa N, Sharma A K, Rao V V R N and Chen W 2014 *Measurement* **47** 33
[21] Nadimicherla R, Kalla R, Muchakayala R and Guo X 2015 *Solid State Ion.* **278** 260
[22] Itoh T, Miyamura Y, Ichikawa Y, Uno T, Kubo M and Yamamoto O 2003 *J. Power Sources* **119** 403
[23] Wen Z, Itoh T, Uno T, Kubo M and Yamamoto O 2003 *Solid State Ion.* **160** 14
[24] Li Q, Sun H Y, Takeda Y, Imanishi N, Yang J and Yamamoto O 2001 *J. Power Sources* **94** 201
[25] Park C H, Kim D W, Prakash J and Sun Y K 2003 *Solid State Ion.* **159** 111
[26] Scrosati B, Croce F and Persi L L 2000 *J. Electrochem. Soc.* **47** 1718
[27] Croce F, Appetecchi G B, Persi L and Scrosati B 1998 *Nature* **394** 456
[28] Liu Y, Lee J Y and Hong L 2003 *J. Appl. Polym. Sci.* **89** 2815
[29] Katsaros G, Stergiopoulos T, Arabatzis I M, Papadokostaki K G and Falaras P 2002 *J. Photochem. Photobiol.* A **149** 191

[30] Magistris A, Mustarelli P, Quartarone E and Tomasi C 2000 *Solid State Ion.* **136** 1241
[31] Xiong H M, Zhao X and Chen J S 2001 *J. Phys. Chem.* B **105** 10169
[32] Singh P K, Bhattacharya B and Nagarale R K 2010 *J. Appl. Polym. Sci.* **118** 2976
[33] Kesavan K, Rajendran S and Mathew C M 2015 *Polym. Compos.* **36** 302
[34] Bahramian A, Raeissi K and Hakimizad A 2015 *Appl. Surf. Sci.* **351** 13
[35] Kumar Y, Hashmi S A and Pandey G P 2011 *Solid State Ion.* **201** 73
[36] Arya A and Sharma A L 2017 *J. Phys. D: Appl. Phys.* **50** 443002
[37] Ramesh S, Winie T and Arof A K 2007 *Eur. Polym. J.* **43** 1963
[38] Younesi R, Veith G M, Johansson P, Edstrom K and Vegge T 2015 *Energy Environ. Sci.* **8** 1905
[39] Mohapatra S R, Thakur A K and Choudhary R N P 2008 *J. Polym. Sci.* B **47** 60
[40] Chung S H, Wang Y, Persi L, Croce F, Greenbaum S G, Scrosati B and Plichta E 2001 *J. Power Sources* **97** 644
[41] Arya A, Sadiq M and Sharma A L 2017 *Ionics* **23** 1–25
[42] Vignarooban K, Dissanayake M A, Albinsson I and Mellander B E 2014 *Solid State Ion.* **266** 25
[43] Mihaylova M D, Krestev V P, Kresteva M N, Amzil A and Berlinova I V 2001 *Eur. Polym. J.* **37** 233
[44] Nimah Y L, Cheng M Y, Cheng J H, Rick J and Hwang B J 2015 *J. Power Sources* **278** 375
[45] Hodge R M, Edward G H and Simon G P 1996 *Polymer* **37** 1371
[46] Liu J W, Li X H, Wang Z X, Guo H J, Peng W J, Zhang Y H and Hu Q Y 2010 *Trans. Nonferr. Met. Soc. China* **20** 344
[47] Ramesh S and Arof A K 2001 *J. Power Sources* **99** 41
[48] Yap Y L, You A H, Teo L L and Hanapei H 2013 *Int. J. Electrochem. Sci.* **8** 2154
[49] Liang G, Xu J, Xu W, Shen X, Zhang H and Yao M 2011 *Polym. Compos.* **32** 511
[50] Arya A, Sharma A L, Sharma S and Sadiq M 2016 *J. Integr. Sci. Technol.* **4** 17
[51] Kulasekarapandian K, Jayanthi S, Muthukumari A, Arulsankar A and Sundaresan B 2013 *Int. J. Eng. Res.* **5** 30
[52] Dey A, Ghoshal T, Karan S and De S K 2011 *J. Appl. Phys.* **110** 043707
[53] Barsoukov E and Macdonald J R 2005 *Impedance Spectroscopy: Theory, Experiment, and Applications* (New York: Wiley)
[54] Selvasekarapandian S, Baskaran R, Kamishima O, Kawamura J and Hattori T 2006 *Spectrochim. Acta* A **65** 1234
[55] Chen H W and Chang F C 2001 *J. Polym. Sci.* B **39** 2407
[56] Stephan A M, Kumar T P, Renganathan N G, Pitchumani S, Thirunakaran R and Muniyandi N 2000 *J. Power Sources* **89** 80
[57] Papke B L, Ratner M A and Shriver D F 1981 *J. Phys. Chem. Solids* **42** 493
[58] Sadiq M, Arya A and Sharma A L 2016 *Integr. Res. Adv.* **3** 16
[59] Cimmino S, Di Pace E, Martuscelli E and Silvestre C 1990 *Macromol. Chem. Phys.* **191** 2447
[60] Wieczorek W, Raducha D, Zalewska A and Stevens J R 1998 *J. Phys. Chem.* B **102** 8725
[61] Jakic M, Stipanelov Vrandecic N, Ocelic Bulatovic V and Govorcin Bajsic E 2016 *Chem. Biochem. Eng. Q.* **30** 61
[62] Fekete E and Pukánszky B 2005 *Eur. Polym. J.* **41** 727
[63] da Silva Neiro S M, Dragunski D C, Rubira A F and Muniz E C 2000 *Eur. Polym. J.* **36** 583
[64] Ramesh S, Yahaya A H and Arof A K 2002 *Solid State Ion.* **148** 483
[65] Thakur A K, Pradhan D K, Samantaray B K and Choudhary R N P 2006 *J. Power Sources* **159** 272
[66] Sharma A L and Thakur A K 2010 *Ionics* **16** 339
[67] Mac Callum J R and Vincent C A 1989 *Polymer Electrolyte Reviews* (Berlin: Springer)
[68] Fan L, Dang Z, Wei G, Nan C W and Li M 2003 *Mater. Sci. Eng.* B **99** 340
[69] Arya A, Sadiq M and Sharma A L 2016 *Proc. of Int. Conf. on Condensed Matter and Applied Physics* vol 1728 p 020364
[70] Macdonald J R 1992 *Ann. Biomed. Eng.* **20** 289
[71] Reddy C V, Zhu Q Y, Mai L Q and Chen W 2007 *J. Solid State Electrochem.* **11** 543
[72] Hema M, Selvasekerapandian S and Hirankumar G 2007 *Ionics* **13** 483
[73] Ratner M A and Shriver D F 1998 *Chem. Rev.* **88** 109
[74] Arya A and Sharma A L 2016 *Appl. Sci. Lett.* **2** 72
[75] Ratner M A and Nitzan A 1989 *Faraday Discuss. Chem. Soc.* **88** 19
[76] Pradhan D K, Samantaray B K, Choudhary R N P and Thakur A K 2005 *J. Power Sources* **139** 384
[77] Bhatt C, Swaroop R, Arya A and Sharma A L 2015 *J. Mater. Sci. Eng.* **11–2** 418
[78] Shukla N and Thakur A K 2010 *Solid State Ion.* **181** 921
[79] Arya A and Sharma A L 2017 *Ionics* **23** 497
[80] Elashmawi I S and Gaabour L H 2015 *Results Phys.* **5** 105
[81] Sharma A L and Thakur A K 2015 *Ionics* **21** 1561
[82] Sharma A L and Thakur A K 2011 *Ionics* **17** 135
[83] Arya A, Sharma S, Sharma A L, Kumar D and Sadiq M 2016 *Asian J. Eng. Appl. Technol.* **5** 4
[84] Sadiq M, Arya A and Sharma A L 2017 *Recent Trends Mater. Devices* **178** 389
[85] Ghosh A, Wang C and Kofinas P 2010 *J. Electrochem. Soc* **157** 846
[86] Nadimicherla R, Sharma A K, Rao V N and Chen W 2015 *Ionics* **21** 1587
[87] Evans J, Vincent C A and Bruce P G 1987 *Polymer* **28** 2324
[88] Bruce P G and Vincent C A 1987 *J. Electroanal. Chem. Interfacial Electrochem.* **225** 1
[89] Munshi M Z A, Owens B B and Nguyen S 1988 *Polym. J.* **20** 597
[90] Sharma A L and Thakur A K 2010 *J. Appl. Polym. Sci.* **118** 2743
[91] Croce F, Settimi L, Scrosati B, Zane D, Gallegos A A, Martinez S S and Reyes J L 2006 *J. New Mater. Electrochem. Syst.* **9** 3
[92] Jinisha B, Anilkumar K M, Manoj M, Pradeep V S and Jayalekshmi S 2017 *Electrochim. Acta* **235** 210
[93] Kumar D and Hashmi S A 2010 *J. Power Sources* **195** 5101
[94] Arof A K, Amirudin S, Yusof S Z and Noor I M 2014 *Phys. Chem. Chem. Phys.* **16** 1856
[95] Bandara T M, Dissanayake M A, Albinsson I and Mellander B E 2011 *Solid State Ion.* **189** 63